

FAILURE DETECTION AND DIAGNOSIS IN A
MULTI-MODULE DEPLOYABLE MANIPULATOR SYSTEM (MDMS)

by

ARUN GUPTA

B.Eng., The Maharaja Sayaji Rao University, Baroda, 1985

M.S., Southern Illinois University, Edwardsville, Illinois, 1999

A THESIS SUBMITTED IN THE PARTIAL FULFILLMENT OF
THE REQUIREMENTS FOR THE DEGREE OF

MASTER OF APPLIED SCIENCE

in

THE FACULTY OF GRADUATE STUDIES
(Mechanical Engineering)

THE UNIVERSITY OF BRITISH COLUMBIA
(Vancouver)

June 2008

© Arun Gupta, 2008

ABSTRACT

This thesis focuses on the study of failure detection and identification of an innovative multi-modular robot that has been designed and developed in our laboratory. The interest in this class of manipulators developed after Canada's participation in the development of the international space station. All the existing space based manipulators have exclusively revolute joints, providing rotational motions. However, our laboratory manipulator has combined revolute (rotational) and prismatic (translational) joints in each module. Several such modules are connected in series to form the multi-modular deployable manipulator system (MDMS), as desired. This innovative design has several advantages when compared with its counterparts; for example, reduced singular configurations, reduced dynamic interactions, and improved obstacle avoidance capability for a specified number of degrees of freedom.

Structural failures of a robotic system are critical in remote and dangerous surroundings such as space, radioactive sites or areas of explosion or battle. During the course of a robotic undertaking if there is a malfunction or failure in the manipulator, still one would wish to have the task completed autonomously, without human intervention. A manipulator that accomplishes such tasks has to be highly reliable, safe, and cost effective, and must possess good maintainability and survival rate. In the present thesis, methodology is developed for identification of structural failures in the multi-modular manipulator system MDMS, which through the use of a decision-making strategy, effective control and kinematic redundancy is capable of satisfactorily executing the intended task in the presence of joint malfunction or failure. The Bayes hypothesis testing method is used to identify the failure. First, a possible set of failure modes is defined, and a hypothesis is associated with each considered failure mode. The most likely hypothesis is selected depending on the observations of the response of the manipulator and a suitable test. This test minimizes the maximum risk of accepting a false hypothesis and thus the identification methodology is considered as most optimal. This failure identification methodology is general and can be used for any failure detection strategy. In the present thesis, the physical MDMS is subjected to several critical failure scenarios in our laboratory. In particular we consider failure due to locked joint, freewheeling of the joint and the sensor failure. The results are studied to evaluate the effectiveness of the methodology for fault-tolerant operation of a class of robotic manipulators.

TABLE OF CONTENTS

ABSTRACT	ii
TABLE OF CONTENTS	iii
LIST OF FIGURES	v
LIST OF SYMBOLS	vi
ACKNOWLEDGEMENT	ix
CHAPTER 1 INTRODUCTION	1
1.1 Preliminary Remarks	1
1.2 Objectives	3
1.3 Review of Literature	6
1.4 Scope of the Investigation	9
CHAPTER 2 EXPERIMENTAL ROBOTIC SYSTEM	11
2.1 Introduction	11
2.2 Physical Robotic System	12
2.3 Design Requirements and Criteria	17
2.4 Computer Control System	19
2.4.1 Optical Encoders	19
2.4.2 Motion Control Interface Board	21
2.4.3 Servo Amplifiers and Power Supplies	22
2.4.4 Control System	22
2.5 Advantages	24
2.6 Manipulator Model	26
CHAPTER 3 STRUCTURAL FAILURE DETECTION	30
3.1 Introduction	30
3.2 Bayesian Hypothesis Testing	31
3.2.1 Gaussian Problem	34
3.3 Joint Failure Modes	38
3.3.1 Sensor Failure	38
3.3.2 Locked Joint Failure	38
3.3.3 Freewheeling Joint Failure	39

CHAPTER 4	FAULT DIAGNOSIS AND CONTROL.....	40
4.1	Introduction.....	40
4.2	Joint Failure Identification.....	40
4.2.1	No Failure.....	40
4.2.2	Sensor Failure.....	42
4.2.3	Locked Joint Failure.....	43
4.2.4	Free Wheeling Joint Failure.....	48
4.2.5	Prismatic Joint Locking Failure.....	52
4.3	Discussion of the Results.....	56
CHAPTER 5	CONCLUDING REMARKS.....	57
5.1	Significance of the Work.....	57
5.2	Main Contributions.....	58
5.3	Summary and Conclusions.....	59
5.4	Recommendations for Future Work.....	60
BIBLIOGRAPHY.....		62
APPENDIX I.....		65

LIST OF FIGURES

Figure 1-1: Canadarm	2
Figure 1-2: Shell Pump in California	2
Figure 1-3: ASIMO by Honda.....	2
Figure 2-1: MDMS Mobile Base	13
Figure 2-2: Schematic Layout of MDMS.....	14
Figure 2-3: AUTOCAD Layout of MDMS	15
Figure 2-4 : The MDMS System Developed in Our Laboratory.....	16
Figure 2-5: Servo Control System Schematic	20
Figure 2-6: Schematic Diagram of the Robot Control System.....	23
Figure 2-7: Underground Arm by Numet Engineering.....	25
Figure 2-8: Hydraulic Excavators.....	25
Figure 2-9: Forestry Equipment.....	26
Figure 2-10: Schematic diagram of the two-module manipulator	28
Figure 3-1: Fault Diagnosis and Control System Block Diagram.....	37
Figure 4-1: Joint Responses Under Normal Operation.....	41
Figure 4-2: Tip Trajectory of the Manipulator Under Normal Operating conditions.....	42
Figure 4-3: Manipulator Response Under Sensor Failure	43
Figure 4-4: Manipulator Response Under Locked Joint.....	45
Figure 4-5: Trajectory of the Manipulator Tip	46
Figure 4-6: Manipulator Response Under Locked Joint 1	47
Figure 4-7: Manipulator Response Under Freewheeling of Base Link.....	49
Figure 4-8: Tip Trajectory of the Manipulator	50
Figure 4-9: Manipulator Response Under Freewheeling of Joint 1.....	51
Figure 4-10: Tip Trajectory of the Manipulator	52
Figure 4-11: Manipulator Response Under Failure of the Base Link Prismatic Joint.....	53
Figure 4-12: Tip Trajectory of the Manipulator	54
Figure 4-13: Manipulator Response Under Failure of the Prismatic Joint of Link 1	55
Figure 4-14: Tip Trajectory of the Manipulator	56

LIST OF SYMBOLS

B	risk function
C	discrete system output matrix
C	cost function
C_{ij}	cost of accepting H_i when H_j is true
$f_{y/H_j}(\mathbf{y} / H_j)$	conditional probability density function of the observation vector given that H_j is true
\mathbf{F}	vector containing the terms associated with the centrifugal, Coriolis, gravitational, elastic and internal dissipative forces
g	gravitational acceleration
H_i	i^{th} hypothesis
\mathbf{K}_d	derivative gain matrix of the PID controller
\mathbf{K}_i	integral gain matrix of the PID controller
\mathbf{K}_p	proportional gain matrix of the PID or FLT controller
l_i	length of i^{th} link
l_d, l_s	length of deployable and slewing links, respectively
M	number of hypotheses
\mathbf{M}	coupled system mass matrix
$\tilde{\mathbf{M}}$	decoupled system mass matrix
$P(H_i, H_j)$	joint probability that H_i is accepted when H_j is true
$P(H_i / H_j)$	conditional probability of accepting H_i when H_j is true
P_{H_j}	apriori probability of occurrence of H_j
\mathbf{q}	set of generalized coordinates leading to the coupled mass matrix \mathbf{M}
$\tilde{\mathbf{q}}$	set of generalized coordinates leading to the decoupled mass matrix $\tilde{\mathbf{M}}$
\mathbf{Q}	vector containing the external non-conservative generalized forces
\mathbf{r}_i	position vector of the elemental mass dm_i with respect to the frame F_i
R_d	Rayleigh dissipation function for the whole system
\mathbf{R}, \mathbf{R}^c	first velocity transformation matrices

\mathbf{R}^v	second velocity transformation matrix
t	time
\mathbf{u}	control input vector
\mathbf{V}_i	covariance matrix of the hypothesis conditioned measurement error
$\mathbf{y} - \hat{\mathbf{y}}_i$	measurement error
(x_i, y_i)	Cartesian components of \mathbf{r}_i
x_d, y_d	desired target point
$\mathbf{x}(k)$	discrete system state vector
\mathbf{y}	observation vector
$\mathbf{y}(k)$	discrete system observation vector
$\hat{\mathbf{y}}_i$	expected value of the measurement vector conditioned on hypothesis
$\tilde{\mathbf{y}}$	observation estimation error
Z	observation space
Z_i	i^{th} observation subspace

Greek Symbols

α_i	rigid body angular motion of the revolute joint i
β_i	flexibility contribution to angular motion of the revolute joint i
δ_{N+1}	generalized coordinate for the elastic deformation of the payload
ϕ	desired pointing direction
$\Phi(k+1, k)$	discrete system state transition matrix
$\Gamma(k+1, k)$	discrete system input distribution matrix

A dot above a character refers to differentiation with respect to time.

A boldface lower case character denotes a vector.

A boldface uppercase character denotes a matrix.

Subscript ‘ d ’ corresponds to deployable (prismatic) link.

Subscript ‘ s ’ refers to the slewing (revolute) link or a specified coordinate.

Abbreviations and Acronyms

ERA	European Robotic Arm
FDI	Failure Detection and Identification
FLT	Feedback Linearization Technique
ISS	International Space Station
LQR	Linear Quadratic Regulator
MBS	Mobile Remote Base System
MDMS	Multi-Module Deployable Manipulator System
$O(N)$	Order-N
PID	Proportional-Integral-Derivative
ROV	Remotely Operated Vehicles

ACKNOWLEDGEMENT

It is my great pleasure and honour to be part of the esteemed scholars of the Industrial Automation Laboratory of the University of British Columbia, and have an opportunity to work with a pool of intelligent and talented personnel. I wish to sincerely express my appreciation to all those who have helped me directly or indirectly during my efforts of the research.

First and foremost I wish to express my gratitude towards my respected supervisor Professor Clarence W. de Silva for his valuable and thoughtful support, teaching, guidance, friendship and openness throughout my graduate studies. At many stages of my current work, he was the driving force and fuel to my “keep going” status. His availability and continued and far-sighted guidance has been enormously helpful in my work. I must acknowledge his great patience and various encouraging words that helped me and provided me a boost whenever I was about to lose confidence in my abilities. His thorough review and editing contributed enormously to the satisfactory completion of this thesis. I am sincerely thankful and indebted to Prof. de Silva. I have learnt considerably from him in life, and I am fortunate to have an association with him as my teacher, guide and friend. His open door policy facilitated me to visit him at odd hours. His willingness to meet and discuss even on the weekends greatly helped me especially that I had been working during the daytime, in the latter part of the completion of this thesis.

I also wish to extend my thanks to Dr. Ying Wang, a post-doctoral fellow in our laboratory, who was always available to guide me and assist when I needed the help. His knowledge about the laboratory equipments was very helpful. The indirect help provided by Dr. Keung Kenneth Wong, a former doctoral student of our laboratory, is also much appreciated.

It will be unfair not to thank my other colleagues and friends in our research laboratory. They shared their experience and knowledge with me and have thus broadened my horizons.

CHAPTER 1 INTRODUCTION

1.1 Preliminary Remarks

The present thesis focuses on the study of failure detection and identification, and fault tolerant operation of an innovative multi-modular robot, the Multi-modular Deployable Manipulator System (MDMS), which has been designed and developed in our laboratory. In particular, Bayesian hypothesis testing is used to identify the failures in the MDMS. The work has a significant experimental component where the physical MDMS is subjected to several critical failure scenarios in our laboratory. The present work is an extension to the past work in our group, which has used analysis and computer simulation [27].

The physical MDMS was designed and developed in our laboratory (Industrial Automation Laboratory—IAL) at the University of British Columbia. The related interest in the study of robotic arms was generated due to the involvement of Canada in the development of the International Space Station (ISS) in cooperation with other countries. All the existing space based manipulators have exclusively revolute joints, providing rotational motions. However, our laboratory manipulator has combined revolute (rotational) and prismatic (translational) joints in each module. Several such modules are connected in series to form the MDMS, as desired. This innovative design has several advantages when compared with its counterparts. Several traditional robotic systems are presented next. Figure 1-1 presents a picture of Canadarm, which was Canada's first contribution to the ISS. This has a multiple revolute joints each with a rotary (slewing) motion. The robotic pump, shown in Figure 1-2, in a Cartesian manipulator, which has exclusively prismatic joints generating translatory motion. The humanoid robot ASIMO Figure 1-3, which has been developed by the Japanese company Honda, has revolute (slew) joints only. In these examples we observe that the robotic structure provides a single movement (rotational or translational) in each joint/link.

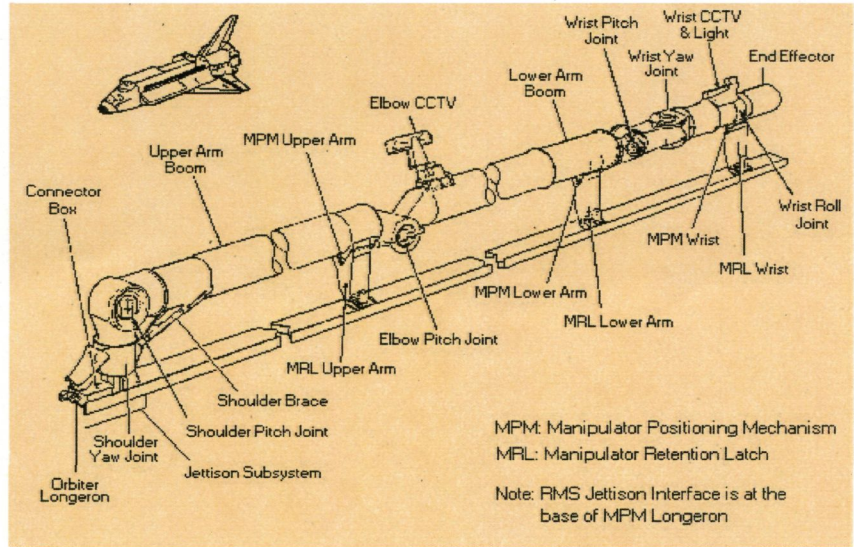
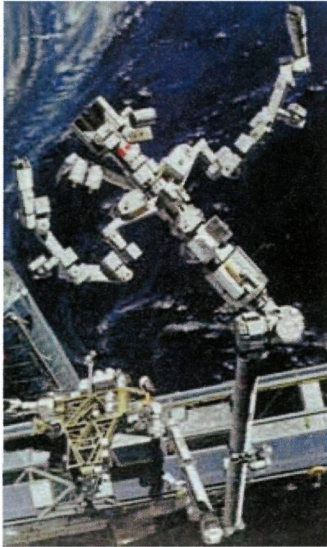


Figure 1-1: Canadarm¹

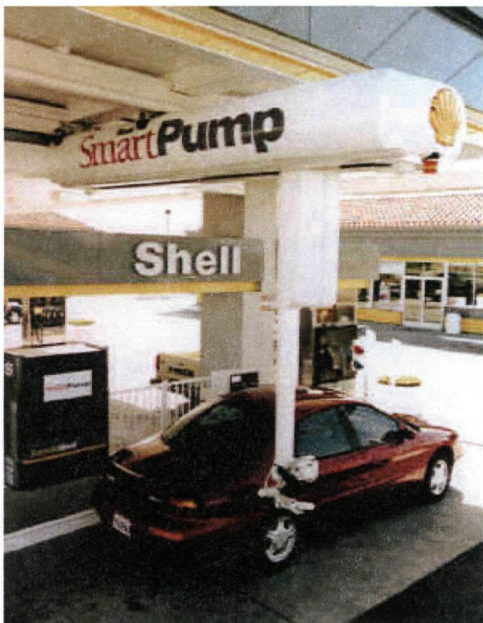


Figure 1-2: Shell Pump in California²

The figure has been removed because of copyright restrictions. The figure is of ASIMO humanoid that has purely revolute joints to manipulate the task. The figure can be found on www.honda.com under Inspiration.

Figure 1-3: ASIMO by Honda

Our laboratory designed and developed model has prismatic (telescopic) movement besides revolute joint movement for each unit. Thus providing two degree of freedom to each unit. It should be noted that revolute-joint manipulators with deployable links (i.e., hybrid manipulators consisting of revolute and prismatic joints) have several advantages.

¹ Courtesy MDA & Canadian Space Agency, 2008

² Courtesy ise.bc.ca ; Reference: ISE

This novel design possesses several attractive features in dynamics and control as it provides reduced number of singular configurations, reduced dynamic interactions and improved obstacle-avoidance capability for a specified number of degree of freedom. The uniqueness of the MDMS, developed in our laboratory is that unlike its counterparts, each module of the arm comprises a revolutes-prismatic joint, providing two types of motion: rotational and translational. The MDMS has been shown to have several advantages over the contemporary manipulators with purely revolutes joints and the same number of links. The main advantages are:

- Simpler decision making requirements
- Reduced inertia coupling or dynamic interaction
- Better capability to avoid obstacles
- Reduced number of singular positions

1.2 Objectives

Research has been performed in our laboratory on the dynamics and control of manipulators, particularly MDMS [21, 6, 28, 4, 11]. Some analytical developments and computer simulations have been done as well on the fault diagnosis of robotic manipulators. The work presented in the present thesis takes a primarily experimental emphasis on the subject of fault-tolerant operation of MDMS.

Consider the failure of one of the joints of a robotic manipulator in the critical task in a space mission or cleaning of a nuclear power plant. The results could be drastic, and as a result it is very critical to study the subject of fault-tolerant operation of robotic manipulators, with the emphasis on taking appropriate corrective action in the event of the failure of one or more joints. The thesis will present the analytical development of an approach for the detection and diagnosis of structural failures of the MDMS. It will describe the physical MDMS and the experimental set up developed in our laboratory for the present investigation. The developed techniques will be experimentally tested to assess their performance.

Fault tolerance in robotics and other automation systems has been gaining attention in the research community. This arises due to the importance of the reliability of equipment as they become increasingly complex, autonomous, and mission critical. The study of fault diagnosis can be categorized into three basic areas: fault detection, fault identification, and system recovery. The desirable objective is to detect and identify a fault or a failure mode in a system and to continue the execution of the specified tasks in a satisfactory manner without the need of human intervention. This ultimately results in higher system reliability, better maintainability, improved survivability, increased efficiency, and greater cost effectiveness.

There are several types of structural failure of robotic manipulators, which are important in the present study, including total failure or partial failure. In particular,

The total failure may result due to:

Locked joint – as a result of jamming of bearings and or transmission

Free swinging of a joint – as a result of breakage of gears, disengagement of transmission, etc.

The partial failure may result due to:

Slip in joint coupling – as a result of increased backlash, partial disengagement of transmission, wear out or any malfunction

High resistance in joint motion – due to misalignment in transmission and/or bearings, lubrication, wear and tear, etc.

Increased vibration – due to backlash in gears, malfunction of gear, bearings, etc.

The method of failure identification that is used in the present is based on Bayes hypothesis testing. First, a possible set of failure modes is defined, and a hypothesis is associated with each considered failure mode. The most likely hypothesis is selected depending on the observation (sensor-based monitoring) of the actual response of the manipulator, and application of a suitable test. The test minimizes the maximum risk of accepting a false hypothesis, and accordingly the identification methodology is considered optimal. The developed failure identification methodology is a general one and any structural failure mode may be included in the detection strategy. The objective of satisfactorily completing a given robotic task is achieved through analytical modeling, control and failure identification methodology, which are somewhat general.

Robotic manipulators play an important role in space exploration and various other critical operations such as cleaning of radioactive locations and similarly hazardous environments. Due to advancements in the robotic technologies and as the required robotic task becomes more critical, the system reliability becomes increasingly important. The need for fault tolerance in the field of robotics is gaining increased attention in the research community. Most space manipulators in use like Canadarm and Canadarm2 that have seven degrees of revolute mobility and working in three-dimensional space it has one redundant degree of mobility for performing an intended task. Similarly many other manipulators have revolute joints only and possess kinematic redundancies.

The main objective of the present thesis is to carry out an experimental investigation of structural failure identification and fault-tolerant control of the MDMS developed by us. Modes of structural failure of the MDMS will be studied, a method of failure diagnosis will be applied, and experiments will be carried out to study the identification of these modes of failure. The cases considered are failure of revolute joint or prismatic joint, and sensor failure. The prototype MDMS in our laboratory consists of four modules connected in series. Each module has an integrated revolute and a prismatic joint and is free to move in the horizontal plane. As a result it possesses eight degrees of freedom. In order to locate a general point in a plane only two generalized coordinates (or degrees of freedom) are required. Furthermore, to orient the end effector on the plane, an additional degree of freedom is needed. Hence there are five degrees of kinematic redundancy in the manipulators. This redundancy can be used to optimize a design criterion such as handling of singularity, avoiding of obstacles, minimization of reaction forces, torques and dynamic interactions, and so on [9]. Another advantage of redundancy is coping with structural failures in robotic joints. This is very important requirement in space missions as it is very difficult to carry out repairs on a space robot once it is launched. Similar problems are faced when working with a faulty robot in a hazardous environment. Hence it is very imperative that methodology is in place to correctly and quickly identify any existing failures of a robotic manipulator, take appropriate corrective actions, and complete the robotic task through proper control possibly with the remaining redundant degrees of freedom without the requirement of human intervention.

In view of these considerations, it is imperative that we gain confidence in the MDMS designed in our laboratory, before it can be used in a practical environment. The simulation study that was conducted out in [27] has been an important step in this

direction. In particular, it has been shown through computer simulation that the MDMS is able to attain the target position in case of a failure. However, it is necessary to take it a step further, implement the methodology of fault tolerance in the physical MDMS, and test its performance under realistic practical scenarios. This is the focus of the present thesis. In reality, the physical manipulator system will be out in the field and exposed to hazards that may be unknown or incompletely known, which could malfunction or failure of one or more of the robot movements.

In the present work, it is attempted to achieve the fault tolerance of physical robots having some level of kinematic redundancy by implementing an affective method of fault diagnosis and a complementary method of control and operation in the presence of partial failure. The important failure modes have been identified previously. In the current study, the real failure modes such as sensor failure, locking of joint and free wheeling caused by power snap due to say entanglement of wires, are incorporated. The connecting wires can get snapped resulting in a disruption of electrical power for the robot. By causing each mode of failure that is considered in the present study, it is found that the earlier results of computer simulation are not valid in some situations. That is, the manipulator system is able to achieve the target, under failure, only in some cases. As a result, acceptable performance of faulty manipulators cannot be guaranteed in totality, even with good control. Further analysis, testing, and enhancement will be required, perhaps in relation to other failure situations. The present study gives a better insight into the physical manipulator system, MDMS, which will contribute toward fault tolerant operation of the system under different scenarios of operation.

1.3 Review of Literature

For many decades, scientists have been studying the role of robotic models in various applications, including space-based robotics. Several groups have carried out research on the dynamics and control of orbiting platform-based manipulators since the late 1970s. De Silva studied a kinematically redundant manipulator, which can optimize its performance in space applications, in the 1980s [9]. Maron and Modi proposed a new design of manipulator with combined movement of slew and deployment similar to the one in the present study in the 1990s [19]. Planar dynamics and control of a single-unit mobile manipulator with rigid links and flexible joints, located on an orbiting flexible platform, have been investigated. Results have shown significant coupling effects

between the platform and the manipulator dynamics. Control of the system during tracking of a specified trajectory, using the computed torques technique, proved to be quite successful. Modi et al. [21] and Hokamoto et al. [14, 15, 16] extended the study to the multi-module configuration, referred to as the Variable Geometry Mobile Manipulator and the Mobile Deployable Manipulator System, respectively. The model includes an arbitrary number of modules and accounts for flexibilities in the joints as well as the links. A relatively general formulation for three-dimensional dynamics of the system in orbit was the focus of the study by Modi et al., while Hokamoto et al. explored a free flying configuration. More recently, Hokamoto et al. [13] studied the control of the Mobile Deployable Manipulator with an arbitrary number of modules, each with two flexible links: one of them free to slew and the other deployable. They developed a numerical procedure for the inverse kinematics of the system and demonstrated that trajectory control of the end-effector using the resolved acceleration approach was quite successful even in the presence of flexibility. Pradhan et al. [22] reported an elegant procedure for the $O(N)$ formulation describing the three-dimensional motion of a system, in a tree topology, using the Lagrangian approach. The objective was to reduce the number of operations needed for the dynamic computations of an N -joint manipulator to be linear in N . Caron extended the $O(N)$ procedure to account for system flexibility as well as deployable links, and applied it to study planar dynamics as well as control of a formidable multi-module deployable manipulator system [5]. The dynamical parametric study in [6] clearly showed complex interactions between flexibility, librational dynamics, and manipulator manoeuvres. Dynamicists have been consistently interested in the discretization procedure that would satisfactorily capture the effect of system flexibility. Zhang et al. [28] attempted to address this issue by:

- Assessing the effect of the number of modes on the response of a single module manipulator, located on an orbiting flexible platform, during a prescribed manoeuvre;
- Studying the effects of variation in flexibility of the revolute joints as well as slewing and deployable links;
- Varying the speed of manoeuvre.

Results showed that the fundamental mode of vibration was able to capture the system response quite accurately. The joint flexibility as well as the speed of manoeuvre

substantially affected the system response. However, the effect of link flexibility was relatively negligible. Of particular significance is the recent contribution by Chen [7]. For the first time he developed an $O(N)$ formulation for the three-dimensional dynamics of an orbiting flexible manipulator, with an arbitrary number of modules, traversing a flexible platform. He illustrated the application of the formulation by studying the dynamics of a multi-module system in the plane of the orbit. Control of the rigid degrees of freedom for a single-module manipulator using the Feedback Linearization Technique (FLT) was also investigated.

The use of kinematic redundancy of a space manipulator for the minimization of dynamic interactions and particularly the loads transmitted between the manipulator base and the space structure has been analytically developed and verified by De Silva [9]. His method uses proper design of the trajectory of the robot and the formulation of the inverse kinematics of a general redundant manipulator, to minimize the loads transmitted between the manipulator and the supporting structure. The approach has been applied to a practical space manipulator system. The FLT is a very popular approach for the control of highly non-linear systems over a large operating range. Applications of this approach to robotic manipulator has been formulated and demonstrated by de Silva and MacFarlane in the 1980s [10]. Subsequently, De Silva developed a computationally efficient recursive approach based on FLT to linearize and decouple a manipulator system for effective control [8].

With respect to the failure in a robotic system, Ting et al. investigated internal shock phenomena due to the failure of joint actuation and a recovery algorithm for both serial and parallel mechanisms under such circumstances [25]. The recovery algorithm generated attempts to reduce the internal shock at the time of failure. Alekseev et al. applied an observer-based approach to solve the problems of on-line failure detection in thrusters and sensors of remotely operated vehicle (ROV). A bank of single-output reduced-order adaptive observers was used, with each observer estimating only one measurable variable whose real value was obtained by using the actual sensor under diagnosis [1]. Kimura et al. in 1998 suggested an autonomous control algorithm for hyper-redundant manipulators that use parallel processing with low performance processors to achieve adaptation to partial failure in space robotics [18]. Here several manipulator joints were locked at a certain angle, in computer simulation, and the adaptability of the control algorithm to these failures was assessed. It was found that a

positioning task could be completed with the control algorithm and the success rate was more than 90%. In the years to come Shin and Lee presented a fault detection strategy and a robust fault recovery control scheme for robot manipulators to overcome actuator failures [23]. The free-swinging joint failure that caused loss of torque at the joint was considered. To identify faults in a wheeled robot, Goel et al. proposed a method of adaptive estimation. It predicted the outcome of several faults and collectively learnt about the failure pattern [12]. Each of the multiple parallel Kalman Filter (KF) estimators was tuned to a particular fault and predicted the expected values for the sensor readings. The difference between the estimated signals and the actual sensor readings was processed by a back propagation neural network [2] and the relevant fault was identified.

1.4 Scope of the Investigation

The objective of the current thesis is to study failure detection and identification and fault tolerant operation of an innovative multi-modular robot, the MDMS. In particular, Bayesian hypothesis testing is used to identify the failures in the MDMS. The work has a significant experimental component where the physical MDMS is subjected to several critical failure scenarios in our laboratory. The present work is an extension to the past work in our group, which has used analysis and computer simulation [27].

The prototype of the MDMS with four modules has been designed and developed in our laboratory. The computer simulations have been carried out for MDMS based on a general system model of a serial manipulator system with an arbitrary number (N) of modules. Each module in the manipulator is capable of performing both revolute (angular motion) and telescopic (translatory motion) operations. This is achieved by two separate motors one for rotating the link and the other for changing the link length. The automatic control of the manipulator system is carried out by implementing two control methods: proportional-integral-derivative (PID) control and FLT. Proper operation and control are preconditions for intended satisfactory operation of MDMS under structural failure. To achieve this end objective, first the developed control program of the robot is tested and verified. Computer simulations have been carried out with several failure modes; specifically, sensor failure, freewheeling, and locked joint. The performance needs to be studied for its authenticity, particularly requiring experimental investigation under practical, real world scenarios. The stage is set for this in Chapter 1.

In Chapter 2, a detailed study is presented on the robotic model developed in the laboratory. The developed manipulator system has four modules (units) connected in series, each capable of rotating and also providing translatory motion. The MDMS in our laboratory provides planar motions, which can represent operation under zero gravity situations in space. The governing equations of motion for a MDMS using Lagrangian procedure and $O(N)$ approach are outlined.

In Chapter 3, the attention is on the development of a failure detection and identification strategy for the MDMS. It is based on Bayesian hypothesis testing and is combined with a bank of Kalman filters for optimally estimating the response of the manipulator under various failure modes. Analytical development of the approach for failure detection and identification as well as response estimation is presented. Further to this, the numerical models that simulate three different failure modes are obtained.

In Chapter 4, the physical manipulator is tested for real failure scenario and results are studied. This is done with the objective of verifying the results from computer simulations and to gain confidence in the physical robotic system and its control system. It is confirmed that only in some failure modes can the manipulator system successfully complete a targeting and pointing task in the event that a telescopic arm gets locked or in case there is a sensor failure. The implications are addressed.

Chapter 5 is the concluding chapter of the thesis. It summarizes the significance of the thesis, outlines the main contributions, and suggests possible future avenues for further work on the subject.

A bibliography of relevant literature is provided and the parameter values of the physical MDMS are given.

CHAPTER 2 EXPERIMENTAL ROBOTIC SYSTEM

2.1 Introduction

Typically a robot consists of several joints/links, and each joint has one degree of freedom. A joint may provide a rotational (or slew) movement—a revolute joint; or may provide a translatory (or deployable or telescopic) movement—a prismatic joint. When there is a failure in the movement of a joint/link then that link is unable to actively contribute to a specified robotic task. Since a joint corresponds to a degree of freedom, if there are more joints than the number of degrees of freedom needed to carry out a task, the robot is said to have redundant kinematics. If a robot possesses redundant kinematics, if a joint fails, the required movement of the corresponding link can be taken up or compensated by other links, through proper control of the robot.

To reach a target point in a plane only two generalized coordinates or degree of freedom are needed. To position an object in a specified direction on the plane, a further degree of freedom is needed. If a robot has more than three degrees of freedom, the redundant degrees of freedom, for planar tasks, can be used to optimize a design criterion such as singularity handling, joint torque minimization, obstacle avoidance and dynamic interaction minimization. Another criterion that can be handled through kinematic redundancy is adaptation to structural failure, which is the focus of the present thesis. As the manipulators are used in varied environments that could be hazardous or too remote for human access; for example, a “rover” robot on the surface of planet Mars, the required robotic tasks become more and more critical and call for highly reliable robotic manipulators. In the same context, fault tolerant robotic manipulators are desired.

Proper operation and control with capabilities of fault tolerance are the basic requirements for desired performance of the Multi-modular Deployable Manipulator System (MDMS), which has been developed by us in the Industrial Automation Laboratory. Ideally, the MDMS must be able to detect and identify a fault or a failure mode in it and must continue to perform the specified task in a satisfactory manner without the need for human intervention. Experimental investigation of this aspect is the focus of the present thesis. This will result in higher reliability, better maintainability, improved survivability, higher efficiency and cost effectiveness in the MDMS.

2.2 Physical Robotic System

The conventional manipulators have joints/links each with a single degree of freedom. Typically, each link is capable of performing one movement (i.e., one degree of freedom). The working prototype of MDMS, as developed in our laboratory, is different from the conventional types of manipulators. The prototype MDMS has four units or modules, each unit having two joints, one capable of slewing (revolute joint) while the other permitted to deploy and retract (prismatic joint). Thus the model has eight degrees of freedom. This prototype robotic system, complete with its control system, is somewhat unique and is capable of real time control and experimentation. The mobile base of the prototype MDMS is sketched in Figure 2-1. This is similar to moving base such as robotic arm mounted on a space station or satellite. Each unit is provided with mechanisms to achieve telescopic as well slew movements. Each module has two motors to achieve the two movements. The rotational motion is achieved by a revolute joint actuated by a DC servomotor with harmonic drive gearing. This link is hollow and carries another link driven by a second DC motor. This second linear motion of deployment or retrieval of links is performed by this DC motor, which is a ball screw linear actuator within the first link. This way, each single module of the manipulator system is capable of providing both slew motion and deployable (prismatic or telescopic) motion. Each module is supported by a rolling support made up of aluminium plate on which three ball transfers are installed. This facilitates movement of links with minimum friction on the horizontal surface. This also reduces the inertial forces and moment about each revolute joint. The links used are rigid while the revolute joints are known to possess some flexibility due to harmonic drive gearing in the motors. The revolute joint of the next unit of the module is attached to the prismatic joint of the first module. The schematic layout of the manipulator is shown in Figure 2-2. The prototype manipulator that is used in the present study has four modules/units, the AutoCAD version of the layout of which is shown in Figure 2-3.

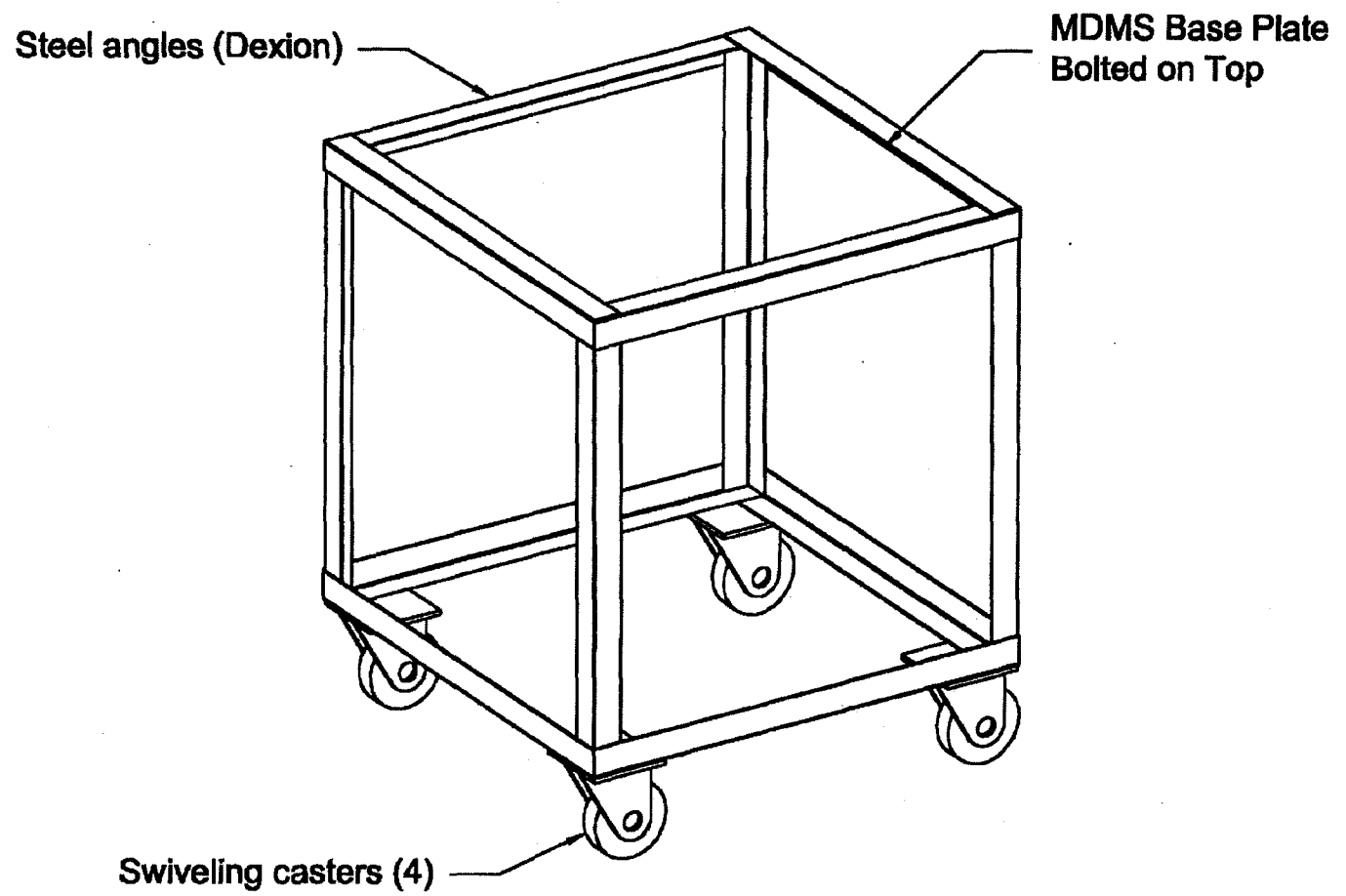


Figure 2-1: MDMS Mobile Base

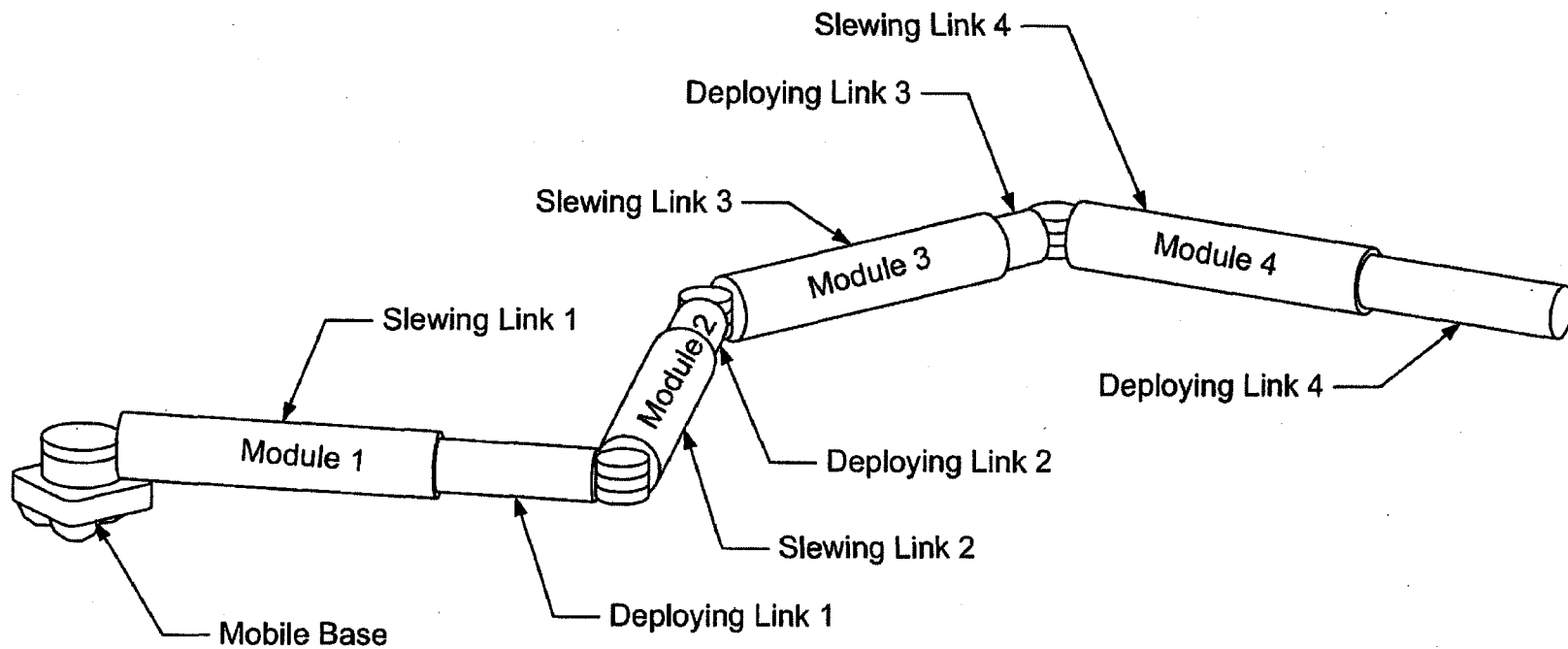


Figure 2-2: Schematic Layout of MDMS

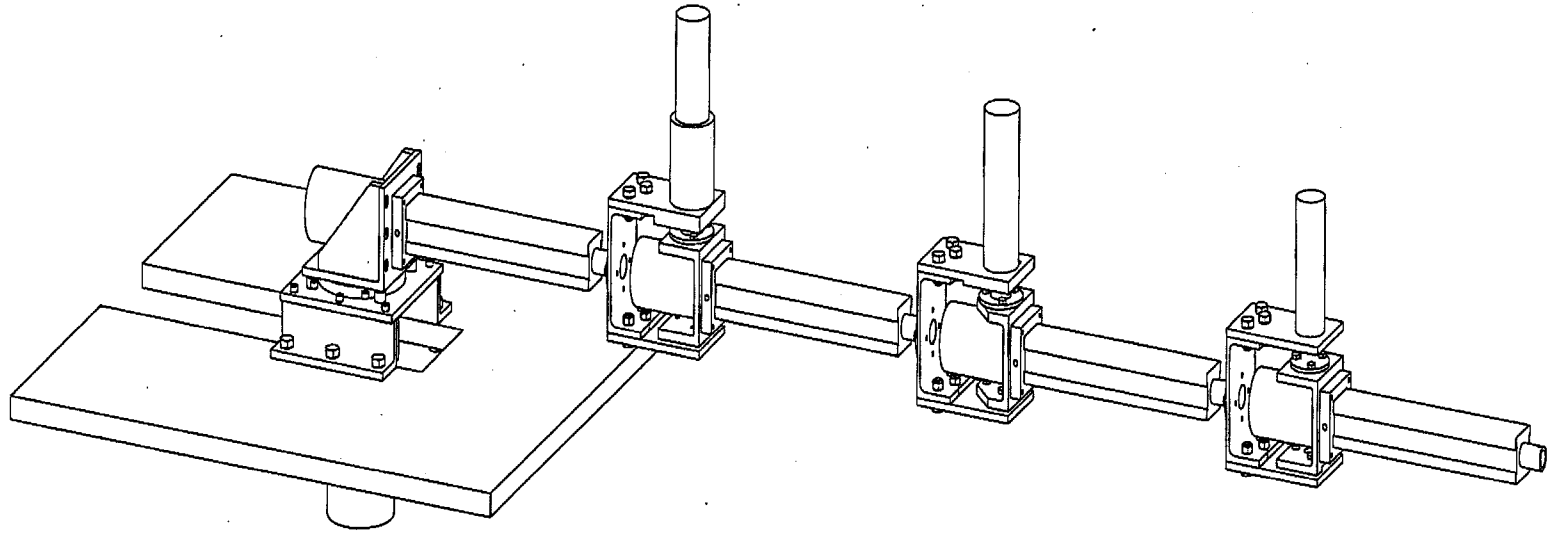


Figure 2-3: AUTOCAD Layout of MDMS

It should be stated that the experiments of the present thesis are carried out using only two modules of the manipulator, operating in the horizontal plane. The system is allowed to move freely on a horizontal plane, and hence the gravitational component of the dynamic forces is zero. This movement can be considered as similar to that in space with zero gravity. Thus this innovative design has received relatively less attention in ground-based applications but has been investigated considerably for space-based applications.

The prototype MDMS designed and developed in our laboratory is shown in Figure 2-4, which consists of four two-degree-of-freedom modules.

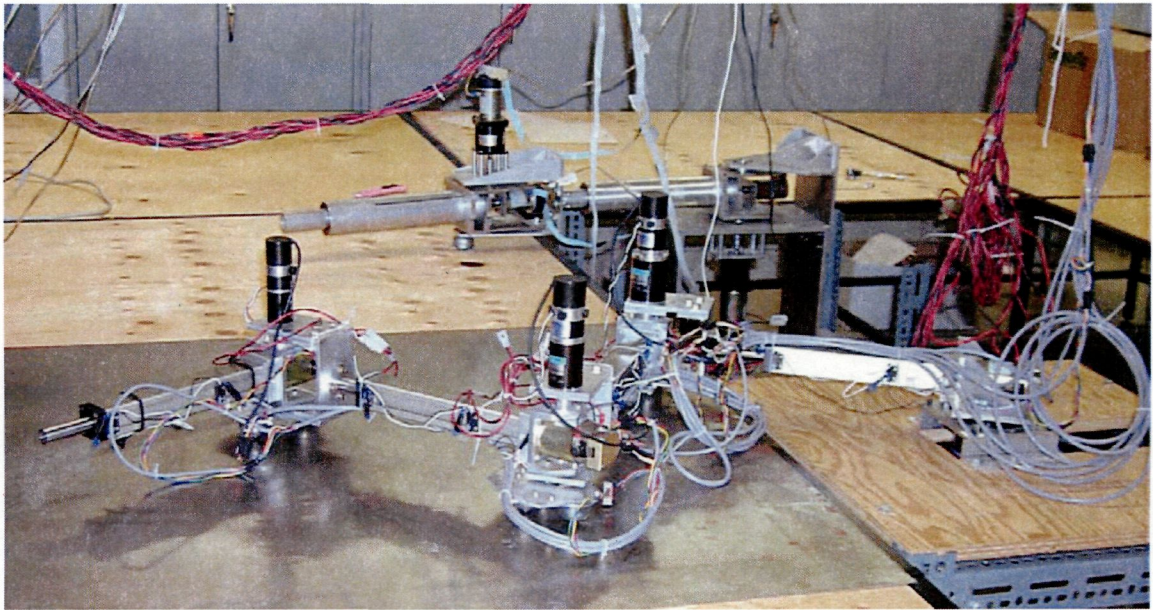


Figure 2-4 : The MDMS System Developed in Our Laboratory

Each manipulator module has a prismatic joint providing translatory movement, and a revolute providing rotary movement. For the experimental studies of the present thesis only two modules are used. Thus the experimental system has four degrees of freedom. To locate the manipulator tip any target point on the task plane, only two degrees of freedom are needed. However, to point the tip of the manipulator in a specified direction in addition to reaching a specified point on the plane, a total of three degrees of freedom are required.

The various parametric values of the constructed prototype manipulator are listed in Appendix I.

2.3 Design Requirements and Criteria

The design requirements for the prototype manipulator developed in our laboratory are:

- Eight-axis planar robotic manipulator with four modules, each consisting of one slewing joint and one deployable joint;
- Full circle slewing motion for the first revolute joint at the base;
- Rolling supports for the manipulator;
- Acceleration of 0.08 m/s^2 at design payload of 5kg;
- Maximum extension of 15 cm for each deployable link;
- Maximum slew speed of $60^\circ/\text{s}$;
- Maximum deployment speed of 4 cm/s;
- PC based system on which different control strategies can be implemented.

With an eight-degree-of-freedom manipulator working in a plane, the kinematic redundancy available to the manipulator would permit satisfactory operation even with joint failure. The rolling supports are important because the length of the manipulator induces a higher loading factor at each unit as well as at the base. This could affect the performance of the actuators, and even damage them. The slew and deployment speeds are comparable to the motions in a space environment.

The basics design criteria are:

- Essentially rigid links;
- Reduced size, weight and inertia compared to a previous two-module version;
- Minimum machining, so that the machine shop time could be minimized;
- Ease of construction and assembly of the modules.

Keeping the rigidity of the links in mind it has been very important to keep the manipulator mass as small as possible. Any additional mass of the system would add to the inertia thus adversely affecting the performance of the system. Besides, the mechanical and electrical components have been chosen based on their performance characteristics like speed, accuracy, reliability and robustness.

The two main parts of the developed prototype robotic manipulator are the manipulator mechanical structure and its control system. The manipulator has been constructed using two types of components:

1. Supplied by outside manufacturers; see Appendix I of [26];

2. Designed and machined in-house in the machine shop of the Department of Mechanical Engineering, University of British Columbia

Basically the prototype manipulator developed by us consists of:

- Rotary actuators with sensors for the revolute joints;
- Linear actuators with sensors for the prismatic joints;
- Rolling supports for the manipulator;
- Test bench for the workspace of the manipulator;
- Bearings and shaft couplings;
- Mounting brackets and connecting components.

The control system comprises:

- Amplifiers and power supplies;
- Motion control interface cards;
- Computer software for programming the controllers (C++).

For our prototype, electric drives were selected compared to hydraulic or pneumatic actuators, as they are lighter and easier to control. In fact in the space-station robot Canadarm, and in many other robotic applications, electric drives are used for revolute joint actuators. Out of the various revolute joint drives available, harmonic drive gearing actuator is selected over other options available. DC servomotor with gearhead has a backlash of about 10 to 20 arc minutes, which contributes to the nonlinearity of the system and challenges the controller. The mounting of a gearhead needs an adapter, which increases the weight and length of the actuator thereby violating the design criterion on the system mass. Direct drive servomotor, however, eliminates the problem of gear backlash and installation complexity. But, their size and weight do not meet the design criteria besides being very expensive, compared to the earlier option. Harmonic drive gearing actuator has various advantages such as zero backlash, high positional accuracy and stiffness. These actuators provide precise motion control and large torque capacity in very compact packages. The integral package contains a servomotor, a harmonic drive gearhead, a tachometer and /or an optical encoder. Furthermore the option of flange output provides a flat surface for mounting the brackets directly to which the deployable link unit can be connected. For prismatic motion, the linear servomotor is good option as it has no backlash because of direct drive operation, smooth motion because of the absence of contacting surfaces to cause friction and stick-slip behaviour; i.e., minimal wear, no need for lubrication, requiring virtually no maintenance. However these motors are intended for high-speed and high-acceleration

applications. Also the assembly requires magnetic iron that defies the design requirements. The linear servomotor has low thrust. In comparison, linear actuators with ball-screws are preferred. It consists of a rotary servomotor, ball-screw and nut, a deploying shaft and an encoder. It is called Pulse Power I (PPI) linear actuator and can apply up to 400 N (90 pounds) of thrust with a standard motor. The model has been constructed with the assistance of highly qualified technicians.

2.4 Computer Control System

The components of the motion control system of the manipulator include an IBM compatible host computer, motion control interface board, power amplifiers, DC servomotors as actuators and optical encoders as feedback sensors. The actuators and optical encoders are connected to the 8-axis ISA bus servo I/O card and amplifiers, which interface the robotic manipulator with a PC compatible computer. This way one can have N modules in the MDMS. Figure 2-5 shows a schematic diagram of the servo control system. Only one axis is shown for clarity. The rationale for selection of specific hardware components is discussed in the following sections.

2.4.1 Optical Encoders

Optical encoders that come integral with the servomotors are used as the feedback devices for the control system. They are digital transducers, thus the analog to digital conversion, which may lead to quantization error, is eliminated. The optical methodology resulting in the no contact feature with rotating discs makes the device durable and almost maintenance free. The output signal from the encoder is available as the number of pulses. It relates to the position of the rotor, and hence the slew motion of the manipulator module as well as the position of the deployable link can be determined. The standard resolution of the unit, with a harmonic drive gearing actuator, is 1000 PPR (pulses per revolution). Since the actuators have the same gear ratio, identical encoders are used for the four revolute joints giving the same resolution at the output shaft.

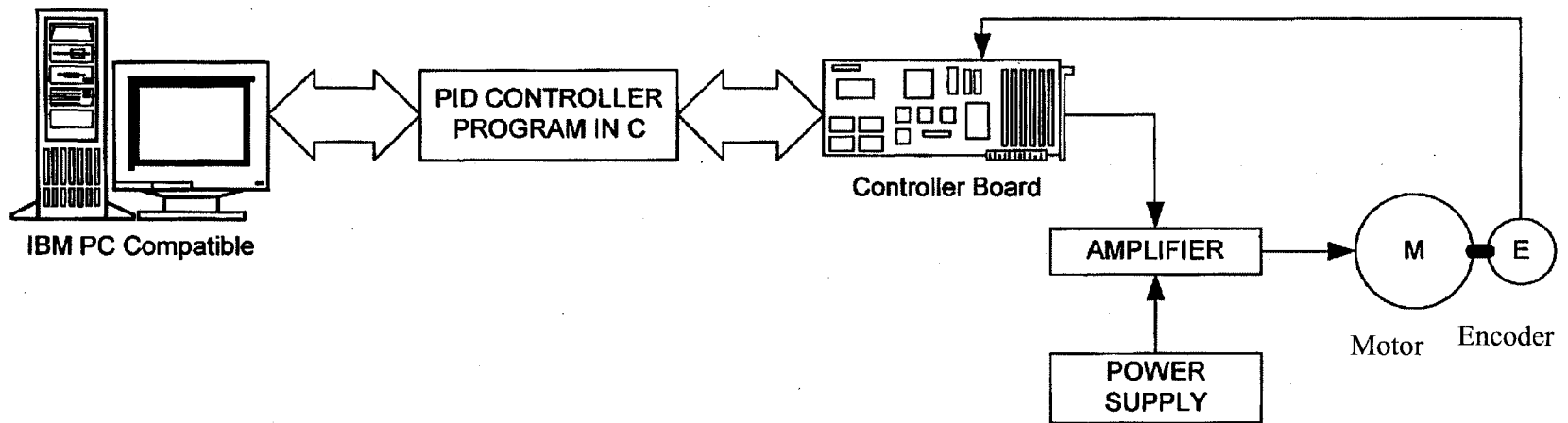


Figure 2-5: Servo Control System Schematic

As for the linear actuators, the standard encoder resolution is 500 PPR. Therefore, with a screw lead of 3 mm, the smallest linear motion that can be measured is 0.006 mm. The signal giving the number of encoder pulses can be measured directly through the quadrature encoder inputs on the motion control interface board.

2.4.2 Motion Control Interface Board

Motion control interface cards, for communications between the manipulator and the computer, are chosen based on the type of actuators and sensors selected for our prototype MDMS. To implement different control algorithms on the prototype robotic manipulator system, an open architecture real-time control system is desired. With the real-time control system, the robotic manipulator will be required to complete certain tasks within a period of time. Therefore, it is important not only to complete the task, but also to perform it within a prescribed time. The two options considered are the motion control interface cards for a digital signal processing (DSP)-based and a PC-based system. With the DSP-based card, a DSP chip or board is required and this would increase the total cost. The processor is used to perform computations necessary to properly control the motor. The conventional thinking has been that the DSP chip is necessary because the main CPU in the PC does not have the processing power to perform the calculations in a reasonable amount of time. This is not true with powerful computers today. Moreover for many applications, an update rate of 1 millisecond is more than sufficient, and this makes an on-board processor unnecessary for most applications.

Based on these considerations, the C-based motion control interface card, MFIO-3A from Precision MicroDynamics Inc. (PMDI) appeared attractive. The MFIO-3A has three channels of 16-bit D/A converters, three quadrature decoder channels, 24 digital I/O channels, a programmable interval timer and a watchdog timer. However, for our 8-axis manipulator system, three MFIO-3A cards would be required. It is desirable to use one board that can provide adequate number of channels rather than having a bank of several cards. After some search, an 8-axis ISA bus servo I/O motion control card from Servo To Go Inc. [Refer Appendix I of 26] was selected. It is a PC based motion control board, which operates on the ISA bus of the computer. This card has similar functionality as the MFIO-3A board, but has more axes and is less expensive. The input/output only approach of this board opens the system to other servo algorithms and control experimentation. With the Windows NT drivers available with the I/O board, the 8-axis ISA bus servo I/O card was selected to operate and control our manipulator in real-time.

2.4.3 Servo Amplifiers and Power Supplies

Servo amplifiers are selected based on the power of the selected servo actuators. Two types of amplifiers were considered: linear amplifiers and pulse width modulation (PWM) amplifiers. The PWM amplifiers were selected because:

- Linear amplifiers are generally more expensive;
- Linear amplifiers are meant for noise sensitive applications;
- PWM amplifiers are technologically more advanced;
- Power wastage, inefficiency, and thermal problems (overheating) are problems for linear amplifiers.

Model 12A8 25A Series servo amplifiers from Advanced Motion Control in Camarillo, CA were selected. These PWM servo amplifiers are designed to drive brushed DC motors. Eight of them are required for our 8-axis manipulator. Series PS1600W unregulated power supply, which is designed to complement the selected amplifiers, was also selected. Two units of power supplies are required since each can operate a maximum of six amplifiers.

2.4.4 Control System

Components of the control system are schematically shown in Figure 2-6. Here S1 and D1 denote the slewing and deployable joints of module 1, respectively. The interface cards between the manipulator and the computer acquire position readings from the encoders, and send them to the control program that generates control actions. The commands are conveyed to the actuators also through the interface cards. The numerical data for the prototype robotic manipulator developed in our laboratory are listed in Appendix I.

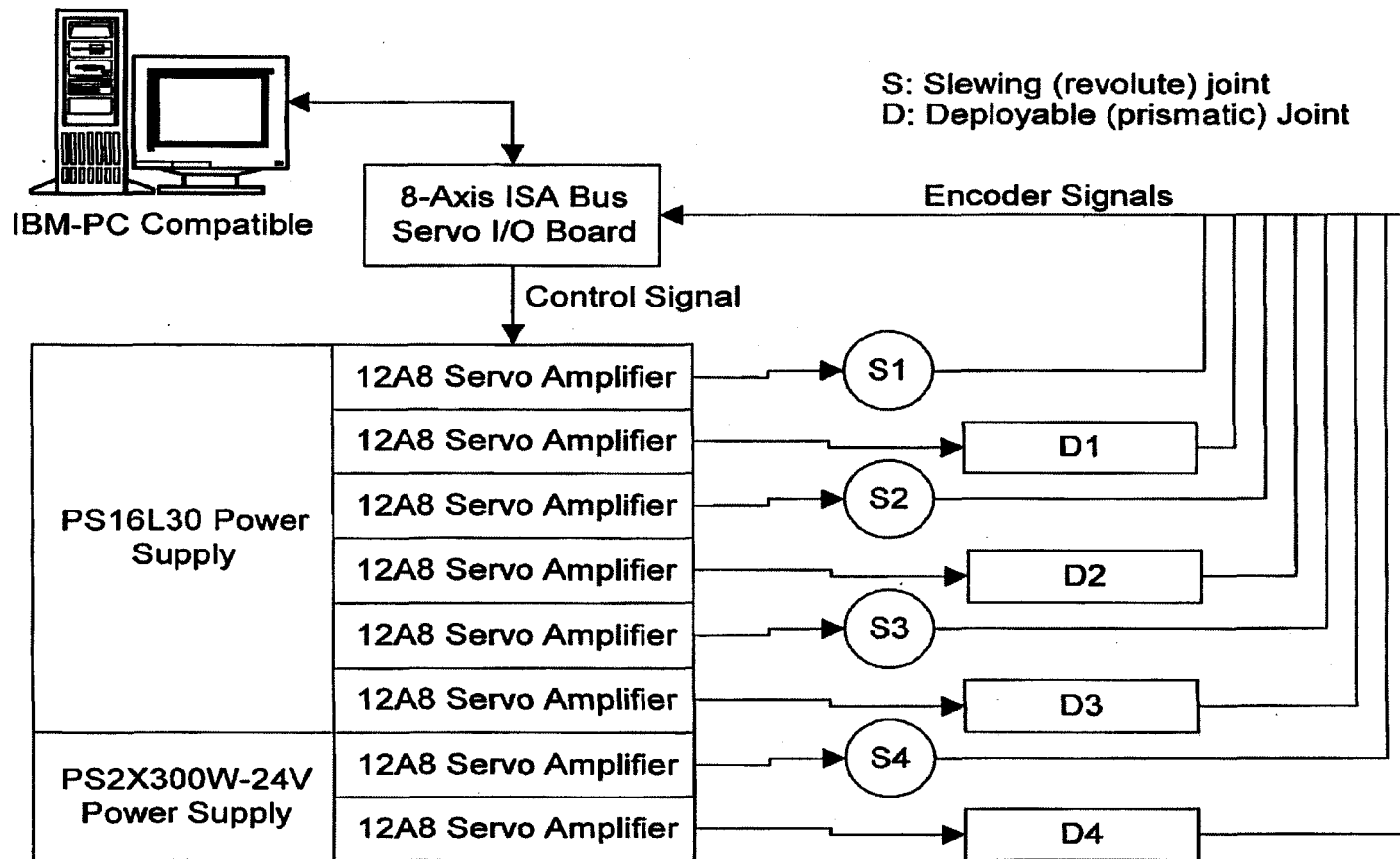


Figure 2-6: Schematic Diagram of the Robot Control System

2.5 Advantages

The prototype robotic system developed in our laboratory, which is under study in the present thesis, has several key features. They are listed below:

- a) The system is ground-based planar robot and has a mobile base.
- b) Each manipulator unit (module) comprises of two links: one link is free to slew (revolute joint) and carries the other link, which is deployable (prismatic joint). The prismatic link is able to deploy and retrieve. The revolute joint of the second module is connected to the prismatic joint of the first module. Each module has two degrees of freedom.
- c) The links are considered rigid while the revolute joint is known to possess some degree of flexibility. The flexibility in the joint is contributed primarily by the harmonic drive gearing in the motor of the revolute joint.
- d) There is damping in the flexible joints and the payload. This may be represented by Rayleigh's dissipation function, in the dynamic model.

The MDMS is characterized by the fact that each module has two degrees of freedom, provided by a revolute joint and a deployable link. This is in contrast to common robotic arms, particularly space-based robots, which have exclusively revolute joints or exclusively prismatic joints. The MDMS is also considered a hybrid manipulator as it possesses both revolute and prismatic joints. They have many important advantages over their contemporary cousins with the same number of links. Some of the advantages are listed below:

- Reduced inertia coupling
- Better capability to avoid obstacles
- Simpler decision making requirements
- Reduced number of singularities

This design idea has been implemented in some practical applications albeit in simplified version. Some of these examples are listed below:

- Underground storage tank telescopic arm by Numet Engineering in Ontario Figure 2-7
- Hydraulic excavators and forestry machineries used by various construction and heavy machinery manufacturers Figure 2-8
- Forestry equipment Figure 2-9

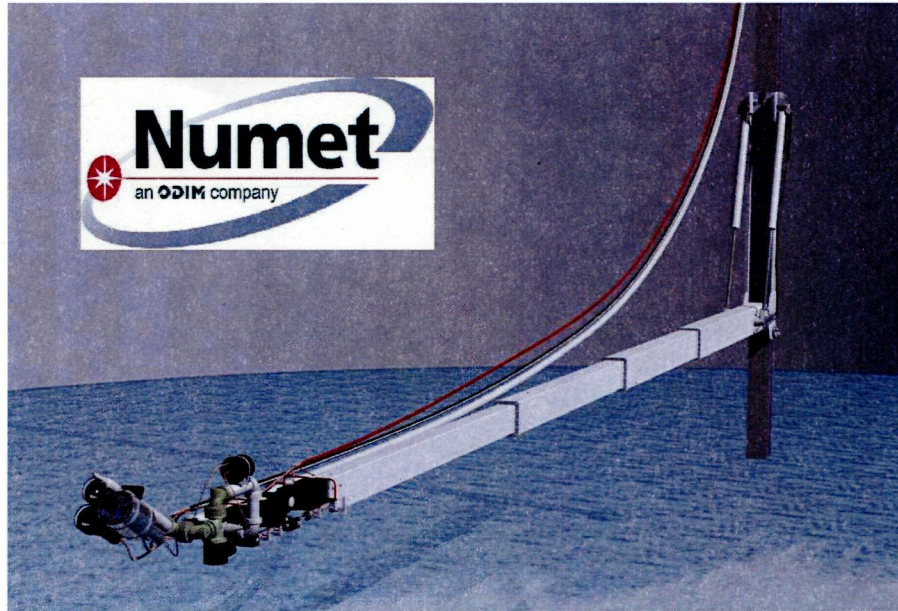


Figure 2-7: Underground Arm by Numet Engineering³



Figure 2-8: Hydraulic Excavators⁴

³ Courtesy www.numet.com

⁴ Courtesy www.volvo.com

The figure has been removed because of copyright restrictions. The figure is of timber handling wheeled forestry equipment that has both revolute and prismatic joints to manipulate the handling. The figure can be found on www.cat.com under forestry equipment.

Figure 2-9: Forestry Equipment

2.6 Manipulator Model

The MDMS developed in our laboratory can benefit from an accurate dynamic model, in its analysis, simulation and control. Such a model has been developed, which is rather general and applicable to a variety of ground-based systems that have fixed or variable link lengths and combinations of revolute and/or prismatic movements. The governing model equations are developed through the Lagrangian approach with specified coordinate motions constrained through Lagrange multipliers. These equations of motions are rather lengthy (depending on the number of manipulator units in the system), highly nonlinear, non-autonomous and coupled. They can be expressed in the general and compact form as

$$\mathbf{M}(\mathbf{q}, t)\ddot{\mathbf{q}} + \mathbf{F}(\dot{\mathbf{q}}, \mathbf{q}, t) = \mathbf{Q}(\dot{\mathbf{q}}, \mathbf{q}, t) \quad (2.1)$$

where $\mathbf{M}(\mathbf{q}, t)$ is the system mass matrix with \mathbf{q} as the vector of generalized coordinates; $\mathbf{F}(\dot{\mathbf{q}}, \mathbf{q}, t)$ is the force vector, which contains centrifugal, Coriolis, gravitational, elastic and internal dissipative forces; $\mathbf{Q}(\dot{\mathbf{q}}, \mathbf{q}, t)$ represents the generalized forces, and contains the control inputs. Equation (2.1) describes the inverse dynamics of the manipulator system. For control and simulation of the system, the forward dynamics is required. For this, equation (2.1) must be solved for $\ddot{\mathbf{q}}$ using

$$\ddot{\mathbf{q}} = \mathbf{M}^{-1}(\mathbf{Q} - \mathbf{F}) \quad (2.2)$$

Solving this equation requires $O(N^3)$ arithmetic operations in the computation of the inverse of the inertia matrix, \mathbf{M}^{-1} , where N is the number of units in the manipulator model system. As can be judged the computational cost for such an operation could be prohibitive for large values of N . In view of this, an $O(N)$ algorithm where the number of arithmetic operations increases linearly with the number of bodies in the system (N) has been developed. This results in much more efficient computation. The coordinates required to describe the system kinematics are taken to be generalized coordinates in order to make the formulation as general as possible. However sometimes it is useful to specify some of these generalized coordinates depending on the executed task.

By the Lagrangian approach, the methodology consists of deriving the system energy using the decoupled set of coordinates \tilde{q} and thereafter converting them into a more convenient coupled set q . Note that \tilde{q} is composed of the inertial positions and orientations and the lengths of the units, the inertial angular position of the rotors in the revolutes joints, and the time dependent generalized coordinates for the transverse elastic displacement of the flexible payload. In obtaining the coupled set of coordinates, the inertial rectilinear position of a unit is converted into the translation of the unit from the tip of the previous unit, and the inertial angular position of a rotor is converted into the angular motion of the rotor with respect to the stator in the revolute joint. The inverse and the time derivative of the mass matrix are computed as:

$$\mathbf{M}^{-1} = \mathbf{R}^{-1}(\mathbf{I} - \mathbf{R}^c) \tilde{\mathbf{M}}^{-1} (\mathbf{I} - \mathbf{R}^c)^T \mathbf{R}^{-T} \quad (2.3)$$

$$\dot{\mathbf{M}} = (\dot{\mathbf{R}}^v)^T \tilde{\mathbf{M}} \mathbf{R}^v + (\mathbf{R}^v)^T \dot{\tilde{\mathbf{M}}} \mathbf{R}^v + (\mathbf{R}^v)^T \tilde{\mathbf{M}} \dot{\mathbf{R}}^v \quad (2.4)$$

In these equations the matrices \mathbf{R} , \mathbf{R}^c , and \mathbf{R}^v are the velocity transformation matrices and $\tilde{\mathbf{M}}$ is the system mass matrix associated with the decoupled set of generalized coordinates. Details of these matrices and the underlying analysis are found in [27]. Note that \mathbf{R} and $\tilde{\mathbf{M}}$ are block diagonal, which are inverted in equation (2.3). Hence their inversion is an $O(N)$ process. Also the structure of the remaining matrices in equation (2.3) allows their multiplication to be of $O(N)$. Thus inversion of the system matrix in terms of the coupled set of generalized coordinates, is now an $O(N)$ process, which is computationally much more efficient.

For the manipulator to recover or properly adapt to any failure mode by successfully identifying the failure, the inverse kinematics of the manipulator is needed. The two-module manipulator has four degrees of freedom. Hence if one of the joints would fail, the manipulator could still complete the task provided that it is achievable with the remaining three degrees of freedom. When a failure is detected in any one of the joints, with the inverse kinematic algorithm a new desired joint trajectory can be computed for the three operational links and provided to the controller. The algorithms for only the no failure and shoulder joint failure mode are presented here.

When both modules of the manipulator system are fully operational, the system needs only three degrees of freedom to reach and orient towards a planar target. The system has one redundant degree of mobility for planar tasks. Rather than tackling the kinematic redundancy of the manipulator system, the length of the first deployable link is fixed. The other three joint variables are then solved geometrically.

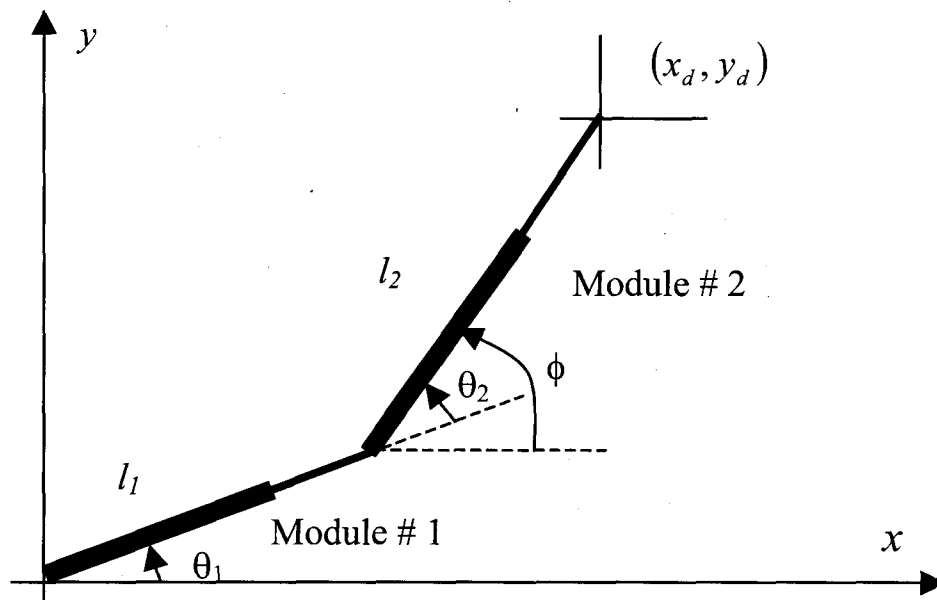


Figure 2-10: Schematic diagram of the two-module manipulator

Figure 2-10 shows a schematic diagram for a two-module deployable manipulator performing a targeting and pointing task. With (x_d, y_d) and ϕ being the desired target and the pointing direction, respectively, and l_1 fixed at an arbitrary value, we can express the joint locus with respect to the manipulator tip as:

$$(x_d - l_2 \cos \phi)^2 + (y_d - l_2 \sin \phi)^2 = l_1^2 \quad (2.5)$$

This is a quadratic equation in l_2 , which may be solved to give

$$l_2 = (x_d \cos \phi + y_d \sin \phi) \pm \sqrt{(x_d \cos \phi + y_d \sin \phi)^2 - (x_d^2 + y_d^2 - l_1^2)} \quad (2.6)$$

$$\theta_1 = \arctan\left(\frac{y_d - l_2 \sin \phi}{x_d - l_2 \cos \phi}\right) \quad (2.7)$$

and

$$\theta_2 = \phi - \theta_1 \quad (2.8)$$

The obvious choice for the possible solution for l_2 is the smaller value, for the reasons of less movement and lower inertia of module # 2, thus less effort for the slew manoeuvre of this module.

Now the inverse kinematics is carried out with the shoulder joint of the two-module manipulator failed. In this case the revolute joint is locked at some position. The manipulator is left with three other degrees of freedom to complete the desired manoeuvre.

When θ_1 is fixed, then in order to achieve the desired orientation, θ_2 has to be equal to $\phi - \theta_1$.

The corresponding deployable lengths of the modules can be computed by expressing the elbow joint coordinates x and y in terms of θ_1 and l_1 , and θ_2 and l_2 , respectively, and equating them to the x and y coordinate expressions:

$$x \text{ coordinate:} \quad l_1 \cos \theta_1 = x_d - l_2 \cos \phi \quad (2.9)$$

$$y \text{ coordinate:} \quad l_1 \sin \theta_1 = y_d - l_2 \sin \phi \quad (2.10)$$

Solving these equations simultaneously yields the expressions for l_1 and l_2 as:

$$l_1 = \frac{y_d - x_d \tan \phi}{\sin \theta_1 - \cos \theta_1 \tan \phi} \quad (2.11)$$

$$l_2 = \frac{y_d - x_d \tan \theta_1}{\sin \phi - \tan \theta_1 \cos \phi} \quad (2.12)$$

CHAPTER 3 STRUCTURAL FAILURE DETECTION

3.1 Introduction

This chapter deals with the development and formulation of the methodology for the detection and identification of structural failure for the multi-modular deployable manipulator system (MDMS). There are several possibilities of structural failure in the MDMS. The failure could be a partial or total. The various scenarios for total failure are:

- Free swinging of a revolute joint or alternatively free sliding of a prismatic joint. This could be due to disengagement of transmission, loss of power, and so on
- Locked joint (rotary or translatory) because of jamming of bearings or transmission or failure of motor in the braked condition
- Failure of data acquisition for a joint
- Sensor failure at joint

The partial failure may occur due to:

- Slippage in a joint. This can be due to increased backlash, partial disengagement of transmission, and wear or malfunction of some part
- Increased resistance in joint movement. This may happen due to the misalignment in transmission or bearing, loss of lubrication, and so on
- Increase in vibration. This can be due to wear, damage, or misalignment of gearing, bearings, and other moving parts.

It is of utmost importance to study these failure modes in order to detect them accurately and quickly during operation of the robotic manipulator. The manipulators under study are useful in remote locations or hazardous environments where it may not be feasible to use humans. Hence the reliability and dependability of these manipulators is of prime importance. The various types of failures listed previously represent some of the common and important failure modes. A robot may get stuck or buried under a heavy load while performing a task. A link may bend or crack due to the impact of a falling or colliding object and may fail to function normally. Containment seals may break and allow dust and contaminants to penetrate into the system thereby causing abrasion of the sliding surfaces, increased friction, and corrosion. In view of all such known and unknown hazards that a manipulator may have to face it is very important that a practical manipulator is thoroughly evaluated using experimentation as well as computer simulation before it is commissioned for a task. In particular, fault tolerance with respect to real failure

scenarios has to be investigated to gain confidence in the system. Through such investigations it is possible to understand the behaviour of the manipulator system under practical conditions and to determine in advance the failure modes under which the manipulator will be able to function adequately and complete the task. Also, one will be able to develop alternative approaches to overcome other failure situations.

The identification of a malfunction or failure involves two tasks; namely, decision and estimation. In the present work the decision of the type of failure that exists is done in an optimal manner on the basis of the cost associated with various decisions that include both correct and incorrect decisions. The development of the failure identification process is based on Bayesian hypothesis testing. The assumption of a Gaussian problem is done in this context. The Gaussian assumption is justified in view of the familiar central limit theorem [2] and it is commonly used in various engineering systems, as in the present work. The formulated decision logic requires the measurement errors and the corresponding covariance matrices, conditioned on each failure hypothesis at each sampling instant. Information on this is obtained by sensing and estimation, through a bank of Kalman filters.

3.2 Bayesian Hypothesis Testing

The main objective of a manipulator system whether fully operational or experiencing some type of malfunction is to detect the operating state and bring the job to a satisfactory conclusion using the detected information and proper control. In the present work, Bayes hypothesis testing is applied to identify the operating conditions of the manipulator, before taking corrective control if a malfunction exists. In the development of Bayes hypothesis testing, first the system is assumed to take one of several, say M , disjoint states each of which is associated with a considered failure mode. Based upon a suitable test and observations, the most likely hypothesis is selected.

The various common tests used for this purpose are:

- Bayes test
- Likelihood ratio test
- Minimax test

The Bayes test is the most general method and the other two are special cases derived from it. In the likelihood ratio test, different hypotheses are given the same apriori probabilities of occurrence. In the minimax test, the maximum risk is minimized. The objective is to find the Bayes risk function corresponding to the least favourable apriori probability distribution. The test is derived using the general Bayesian procedure.

The present method of failure identification is based on Bayes hypothesis testing. First, a possible set of failure modes is defined, and a hypothesis is associated with each considered failure mode. The most likely hypothesis is selected depending on the observations of the response of the manipulator and a suitable test. This test minimizes the maximum risk of accepting a false hypothesis, and accordingly the identification methodology is considered optimal. The general Bayesian hypothesis testing algorithm is derived by first defining M disjoint states or hypotheses, denoted by $H_1, H_2, H_3, \dots, H_M$. The observation space Z is partitioned into M subspaces $Z_1, Z_2, Z_3, \dots, Z_M$. The system is assumed to take one of the several, say M , disjoint states each of which is associated with a considered failure mode. Then the observation space is given as

$$Z = \bigcup_{i=1}^M Z_i \quad (3.1)$$

If the observation vector falls into a particular observation subspace Z_i , then H_i is chosen as the most likely hypothesis. Mathematically, we can state that as

$$\mathbf{y} \in Z_i \Rightarrow \text{accept } H_i \quad (3.2)$$

The subspaces Z_i are determined by minimizing the risk function B , which is defined as the expected value of the cost function denoted by $C(\mathbf{H}, \mathbf{H})$. This cost function specifies the penalty or loss or cost of making an incorrect decision. Here \mathbf{H} denotes the hypothesis set $\{H_1, H_2, H_3, \dots, H_M\}$. Particularly, C_{ij} is the cost of accepting the hypothesis H_i when the hypothesis H_j is actually true. The risk function can be expressed as

$$B = E[C(\mathbf{H}, \mathbf{H})] = \sum_{i=1}^M \sum_{j=1}^M C_{ij} P(H_i, H_j) \quad (3.3)$$

where $P(H_i, H_j)$ is the joint probability that H_i is accepted when H_j is true:

$$P(H_i, H_j) = P(H_i/H_j)P_{H_j} \quad (3.4)$$

and

$$P(H_i/H_j) = \int_{Z_i} f_{\mathbf{y}/\mathbf{H}}(\mathbf{y}/H_j) d\mathbf{y} \quad (3.5)$$

where

$P(H_i/H_j)$ is the conditional probability of accepting H_i given that H_j is true,

P_{H_j} is the apriori probability of occurrence of H_j and $f_{\mathbf{y}/H_j}(\mathbf{y}/H_j)$ is the conditional probability density function of the observation random vector given that B is true.

The substitution of equation (3.5) in equation (3.3) yields,

$$B = \sum_{i=1}^M \sum_{j=1}^M C_{ij} P_{H_j} \int_{Z_i} f_{\mathbf{y}/H_j}(\mathbf{y}/H_j) d\mathbf{y} \quad (3.6)$$

Since

$$\int_{Z_i} f_{\mathbf{y}/H_j}(\mathbf{y}/H_j) d\mathbf{y} = 1$$

we get

$$0 = \sum_{j=1}^M C_{jj} P_{H_j} - \sum_{j=1}^M \sum_{i=1}^M C_{ij} P_{H_j} \int_{Z_i} f_{\mathbf{y}/H_j}(\mathbf{y}/H_j) d\mathbf{y}$$

Thus the risk function may be expressed as

$$B = \sum_{j=1}^M C_{jj} P_{H_j} + \sum_{i=1}^M \int_{Z_i} \left(\sum_{j=1}^M \beta_{ij} \right) d\mathbf{y} \quad (3.7)$$

where

$$\beta_{ij} = (C_{ij} - C_{jj}) P_{H_j} f_{\mathbf{y}/H_j}(\mathbf{y}/H_j) \quad (3.8)$$

The first term on the right hand side of equation (3.7) is a constant and therefore can be disregarded in the minimization. Also from equation (3.8) we see that

$$\beta_{ii} = 0 \quad \text{for all } i \text{ and } \beta_{ij} > 0 \quad \text{for } i \neq j$$

because, for a realistic problem with non-zero probability density functions, there is

$$C_{ij} > C_{ii} \quad \text{for any } i \text{ and all } j \neq i \quad (3.9)$$

and

$$P_{H_j} f_{\mathbf{y}/H_j}(\mathbf{y}/H_j) > 0 \quad (3.10)$$

Thus, the risk function (3.7) can be simplified further as

$$B^* = \sum_{i=1}^M \int_{Z_i} \left(\sum_{j=1, j \neq i}^M \beta_{ij} \right) d\mathbf{y} \quad (3.11)$$

Hence, for a particular observation vector say \mathbf{y} , if the minimum of $\sum_{j=1, j \neq i}^M \beta_{ij}$ corresponds to $i = l$

then we accept H_l as the most likely hypothesis because then and only then each integral in the summation over l will be at its minimum, hence B^* will be minimum.

Suppose that the apriori probabilities of occurrence of different hypotheses are the same; in particular,

$$P_{H_j} = P_H \quad \text{for all } j$$

and the cost of selecting a correct hypothesis is zero:

$$\begin{aligned} C_{ij} &= 0 & \text{for } i = j \\ &= C > 0 & \text{for } i \neq j \end{aligned}$$

Then

$$\sum_{j=1, j \neq i}^M \beta_{ij} = CP_H \sum_{j=1, j \neq i}^M f_{\mathbf{y}/H_j}(\mathbf{y} / H_j)$$

As the minimum of this expression is resulted if and only if the largest term in the summation is eliminated, the decision logic becomes:

$$\text{Accept: } H_l \text{ if } f_{\mathbf{y}/H_l}(\mathbf{y} / H_l) \geq f_{\mathbf{y}/H_i}(\mathbf{y} / H_i) \text{ for all } i \neq l \quad (3.12)$$

3.2.1 Gaussian Problem

The various inputs to the manipulator system and the measurements through the sensors generally contain the disturbances usually in the form of noise. The common assumption is that the disturbances and noise are independent zero mean Gaussian white noise vectors. This common assumption is justified in view of the central limit theorem [2]. If the system initial states are Gaussian, then the state vector is also Gaussian because it is a linear combination of the initial state and the input disturbances. Accordingly, the measurement vector is also Gaussian. Therefore, one has

$$f_{\mathbf{y}/H_j}(\mathbf{y} / H_j) = \frac{1}{(2\pi)^{m/2} |\mathbf{V}_j|} e^{-\frac{1}{2}(\mathbf{y} - \hat{\mathbf{y}}_j)^T \mathbf{V}_j^{-1} (\mathbf{y} - \hat{\mathbf{y}}_j)} \quad (3.13)$$

Here $\hat{\mathbf{y}}_i$ is the expected value of the measurement vector conditioned on hypothesis H_i and \mathbf{V}_i is the covariance matrix of the hypothesis conditioned measurement error $\mathbf{y} - \hat{\mathbf{y}}_i$. Since logarithm is a monotonic function, the test (3.12) is similar to the following:

$$\text{Accept } H_l \text{ if } \ln f_{\mathbf{y}/H_l}(\mathbf{y} / H_l) \geq \ln f_{\mathbf{y}/H_i}(\mathbf{y} / H_i) \text{ for all } i \neq l$$

Applying equation (3.13) results in:

$$\text{Accept } H_l \quad \text{if } \alpha_l \leq \alpha_i \text{ for all } i \neq l \quad (3.14)$$

where

$$\alpha_i = \ln|\mathbf{V}_i| + \frac{1}{2}(\mathbf{y} - \hat{\mathbf{y}}_i)^T \mathbf{V}_i^{-1}(\mathbf{y} - \hat{\mathbf{y}}_i) \quad (3.15)$$

The decision logic developed here requires the information of the measurement errors $\mathbf{y} - \hat{\mathbf{y}}_i$ and the corresponding covariance matrices \mathbf{V}_i conditioned on each hypothesis H_i at every instant when the system is checked for any failure and the decision is made. We can obtain this at either each sampling instant or after we have some accumulated observations. It is desirable to opt for the later as that will produce more accurate decisions, because more information will be available at each hypothesis testing stage. In the present work, a decision is made at every sampling instant. The hypothesis conditioned errors and the covariance matrices are obtained from a bank of M Kalman filters.

Consider a robotic manipulator whose dynamics given by the following discrete state-space equations, which are linearized by expanding the system equation using the Taylor series and neglecting the higher order terms:

$$\begin{aligned} \mathbf{x}(k+1) &= \boldsymbol{\Phi}(k+1, k)\mathbf{x}(k) + \boldsymbol{\Gamma}(k+1, k)\mathbf{u}(k) + \boldsymbol{\Gamma}(k+1, k)\mathbf{w}(k) \\ \mathbf{y}(k+1) &= \mathbf{C}\mathbf{x}(k+1) + \mathbf{v}(k+1) \end{aligned} \quad (3.16)$$

Here \mathbf{w} and \mathbf{v} are independent zero mean Gaussian white noise processes so that

$$E[\mathbf{w}] = 0 \quad (3.17)$$

$$E[\mathbf{v}] = 0 \quad (3.18)$$

$$E[\mathbf{w}\mathbf{w}^T] = 0 \quad (3.19)$$

$$E[\mathbf{w}(j)\mathbf{w}^T(k)] = \delta_{jk} \mathbf{Q} \quad (3.20)$$

$$E[\mathbf{v}(j)\mathbf{v}^T(k)] = \delta_{jk} \mathbf{R} \quad (3.21)$$

The initial state vector is a Gaussian process that is independent of the input disturbances and measured noise, and the mean and the covariance matrix are given by

$$E[\mathbf{x}(0)] = \bar{\mathbf{x}}(0) = \mathbf{x}_0 \quad (3.22)$$

$$E[\mathbf{x}(0)\mathbf{x}^T(0)] = \mathbf{P}(0) \quad (3.23)$$

When the set of past observations $\{\mathbf{y}(1), \mathbf{y}(2), \dots, \mathbf{y}(j)\}$ are given, considering the estimate $\hat{\mathbf{x}}(k/j)$ of $\mathbf{x}(k)$, the optimal estimate is obtained by minimizing the cost function

$E[L(\tilde{\mathbf{x}}(k/j))]$. The minimized cost function is expressed as

$$\hat{\mathbf{x}}(k/j) = E[\mathbf{x}(k) / \mathbf{y}(1), \mathbf{y}(2), \dots, \mathbf{y}(j)] \quad (3.24)$$

where $L(\tilde{\mathbf{x}}(k/j))$ is an admissible loss function of the estimation error

$\tilde{\mathbf{x}}(k/j) = \mathbf{x}(k) - \hat{\mathbf{x}}(k/j)$. From equation (3.16), one obtains

$$\mathbf{x}(k) = \Phi(k, j)\mathbf{x}(j) + \sum_{i=j+1}^k \Phi(k, i)\Gamma(i, i-1)[\mathbf{u}(i-1) + \mathbf{w}(i-1)]$$

Taking the conditional expectation of both sides, knowing $\{\mathbf{y}(1), \mathbf{y}(2), \dots, \mathbf{y}(j)\}$ and with the assumption that $\mathbf{w}(i)$ is independent of $\mathbf{y}(j)$ for $i \geq j$, the optimal estimate of (3.24) is obtained as

$$\hat{\mathbf{x}}(k/j) = \Phi(k/j)\hat{\mathbf{x}}(j/j) + \sum_{i=j+1}^k \Phi(k, i)\Gamma(i, i-1)\mathbf{u}(i-1) \quad (3.25)$$

The conditional distribution of a Gaussian random vector \mathbf{x} given another one \mathbf{y} , is Gaussian with mean and the covariance matrix given by the following [20]:

$$E[\mathbf{x} / \mathbf{y}] = \bar{\mathbf{x}} + \mathbf{P}_{xy}\mathbf{P}_{yy}^{-1}(\mathbf{y} - \bar{\mathbf{y}}) \quad (3.26)$$

$$\mathbf{P}_{x/y} = \mathbf{P}_{xx} - \mathbf{P}_{xy}\mathbf{P}_{yy}^{-1}\mathbf{P}_{yx} \quad (3.27)$$

where,

$$E[\mathbf{x}] = \bar{\mathbf{x}}$$

$$E[(\mathbf{x} - \bar{\mathbf{x}})(\mathbf{y} - \bar{\mathbf{y}})^T] = \mathbf{P}_{xy}$$

For Gaussian random vectors \mathbf{x} , \mathbf{y} , and \mathbf{z} one has

$$E[\mathbf{x}/y, z] = E[\mathbf{x}/y, \tilde{z}] = E[\mathbf{x}/y] = E[\mathbf{x}/\tilde{z}] - \bar{\mathbf{x}} \quad (3.28)$$

where

$$\tilde{z} = z - E[z/y]$$

Since $\mathbf{x}(0)$ and $\mathbf{w}(i)$ are Gaussian, $\mathbf{x}(k)$ is merely a sum of Gaussian random vectors, and thus is Gaussian. Similarly, $\mathbf{y}(k)$ is Gaussian as $\mathbf{v}(i)$ and $\mathbf{x}(i)$ are Gaussian.

The operation of this fault diagnosis and control system is shown in the block diagram of Figure 3-1. The desired motion is the reference motion that is fed to the system. The actual robotic motion is compared to the desired motion and is fed to the controller along with the estimated output. The corrected output is then linearized and passed through various Kalman filters. The results are then processed using the failure mode detection logic. Thereafter the output is estimated and compared to the desired output. The PID controller used here controls the manipulator motion so that the estimated output matches the desired output.

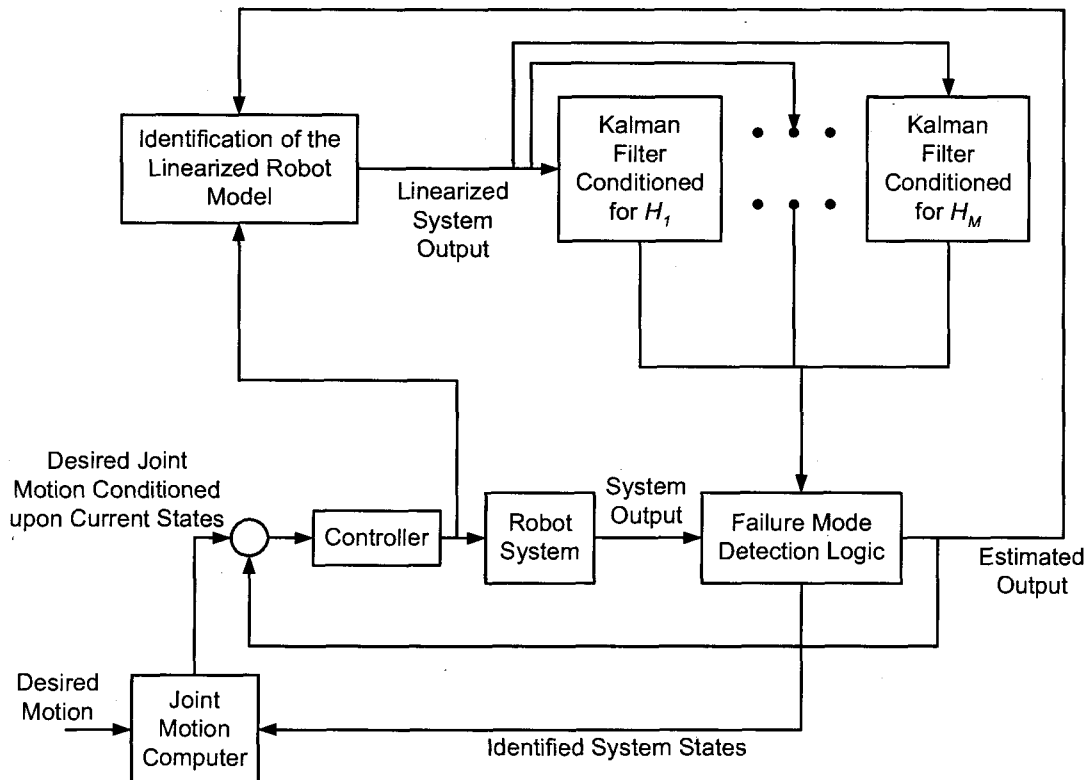


Figure 3-1: Fault Diagnosis and Control System Block Diagram

3.3 Joint Failure Modes

As seen in Section 3.1 there are several failure modes classified as total or partial failure. In the current study, the three main failure modes considered are locked joint, free joint and sensor failure. These are some of the major failure modes. For a manipulator, a revolute joint and a prismatic joint provide the key movements of rotation and translation. The sensor provides the target location. Hence in the present work, the focus is made on the study of failure modes on account of freewheeling, locking of shoulder joint, locking of prismatic joint and sensor failure. The failures can be caused due to various reasons such as those listed in Section 3.1. In the current work we have used situations when a power failure takes place, which is quite convenient to realize in the laboratory set up. Another advantage is that this does not damage the manipulator system. It is to be noted that any other failure mode must be carried out with due care as it may damage the robotic system. The errors and the error covariance matrices conditioned on different hypotheses, which are associated with the considered failure modes, require system models that represent the corresponding failure modes.

3.3.1 Sensor Failure

In this mode, the optical encoder (motion sensor) of a revolute joint or a deployable link fails. In the normal state the optical encoder provides a reading in number of pulses, which correspond to the angular or linear position of the joint. However in the faulty state it is assumed that the sensor gives a zero output though the joint motion continues according to the actuator input signal. In the present study, this was achieved by replacing the row of the measurement (output) matrix corresponding to the sensor that has failed by a null row. The time history graph plotted shows that the magnitude of the count increases with time as the manipulator moves with the constant torque and force applied to the joints.

3.3.2 Locked Joint Failure

Here the relative motion of the joint is stopped due to some form of jamming, power failure, an obstacle, or seizure in a joint component such as the gear transmission or the bearings. Once locked, the position of the locked joint stays the same as that at the instant just prior to the locking, and its relative velocity drops to zero and maintains at this value throughout the locked state. The study was also performed where the translatory motion of the unit was locked. In the present study, this was achieved by reducing the total degrees of freedom of the manipulator system by one, by fixing the generalized coordinate corresponding to the locked joint. In this

manner, the equation corresponding to the coordinate for the locked joint is left out from the original system of nonlinear equations of motion.

3.3.3 Freewheeling Joint Failure

In this failure mode the study is done where there is a free swinging of a revolute joint. This is the result of a loss of connection between the harmonic-drive motor and the slew link. This could be due to a broken link, slipping or disengagement in the transmission or loss of torque in the actuator as a result of malfunction in the drive system or the actuator. When this occurs, the corresponding actuator torque drops to zero, having no effect on the manipulator motion.

CHAPTER 4 FAULT DIAGNOSIS AND CONTROL

4.1 Introduction

In this chapter, experimental investigations are carried out using the physical robotic system multi-module deployable manipulator system (MDMS) to establish the effectiveness of the developed procedure in detecting a set of important failure modes. Also investigated is the effectiveness of the experimental robot in completing a robotic task, under joint failure, by using kinematic redundancy. The results presented in this chapter verify through experimentation the conclusions arrived at, from earlier work by computer simulation [27].

4.2 Joint Failure Identification

The failure mode identification algorithm that uses Bayesian hypothesis testing, as developed, is implemented in the experimental manipulator, MDMS for detecting joint failures. To gain confidence in the operation of the experimental robot developed in our laboratory, in the presence of sensor failure and a locked joint, the algorithm has been tested on a single module of the manipulator, and thereafter on the two-module manipulator. The sampling period for the linearized and discretized models is chosen to be equal to the control time step. The outputs that are measured in the present study are the position for the revolute and prismatic joints. They are measured with the optical encoders mounted on the joint motor shafts. The inputs to the manipulator are the forces and torques provided to the motors.

In the current study, the following four hypotheses are investigated through experimentation:

1. H1: No failure
2. H2: Sensor failure
3. H3: Locked joint
4. H4: Free joint

The matrix \mathbf{R} in equation (3.21) is selected such that there is a higher noise covariance associated with a failed sensor. The actual value of \mathbf{Q} in equation (3.20) and \mathbf{R} depend on the sensors used and the engineering units that vary from one system to another.

4.2.1 No Failure

Necessarily, the case where there is no failure is also one of the hypotheses that is tested. This is in fact the normal state when the manipulator is functioning properly. The revolute joint for the base link, after initial fluctuations, reaches the steady state. A similar pattern is observed for joint one of the manipulator. The prismatic joints in both cases extend to the desired level to reach the

target point. The experimental results are plotted in Figure 4-1 for each link. It is seen that each joint motion attains the steady state, as required. The velocity curves for the revolute joints, after initial disturbance, attains the equilibrium state and reaches the steady state when reaching the target. The revolute joints attain the normal state and the prismatic joint extends to reach the target point, under PID control.

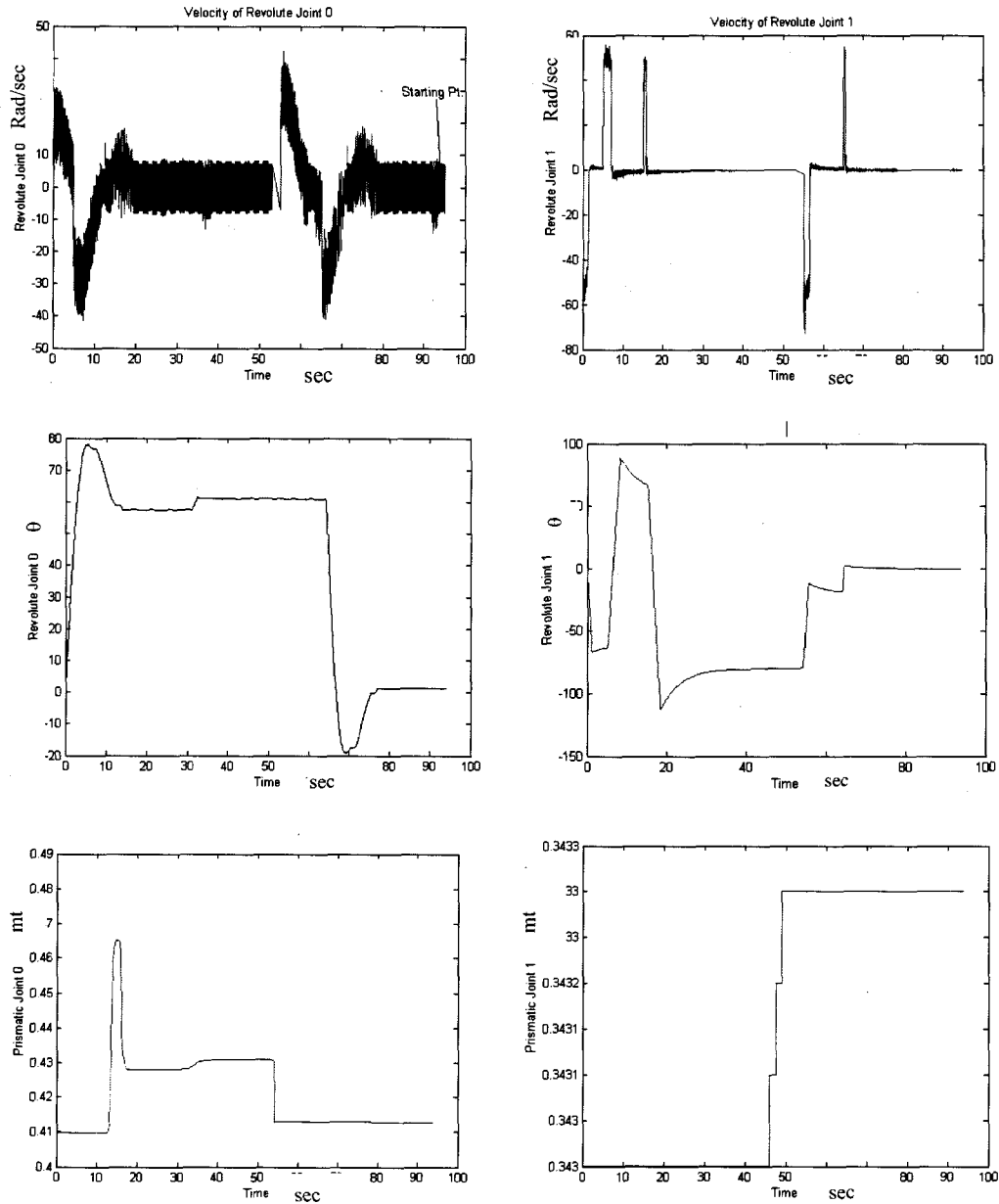


Figure 4-1: Joint Responses Under Normal Operation

The trip trajectory of the robot, under normal operation corresponding to Figure 4-1, is shown in Figure 4-2. It is seen that a desired target is reached while initial motions of the tip fluctuation are suppressed by PID controller. Compensation for the inertial forces and the torque has been required to correctly achieve the target. This gives us the confidence in the proper function of the physical manipulator and its control hardware and software, under conditions of normal operation.

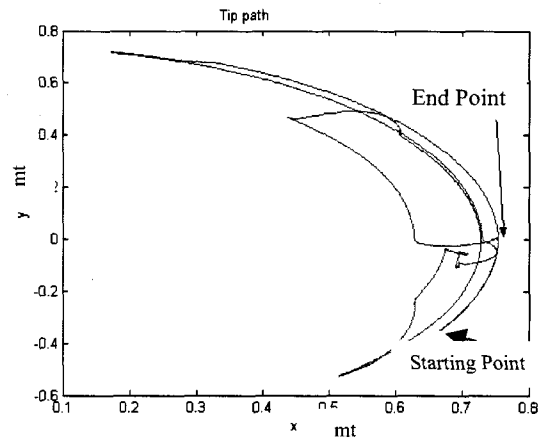


Figure 4-2: Tip Trajectory of the Manipulator Under Normal Operating conditions

4.2.2 Sensor Failure

In the mode of sensor failure, the optical encoder of a revolute or deployable joint is considered to fail. In normal operation, these encoders provide a reading in terms of pulses that correspond to the angular or linear position of the joint. In the case of a sensor failure the corresponding sensor provides a zero output reading although the joint motion continues according to the actuator input signal. In simulation studies [27] the row of the measurement matrix C corresponding to the failed sensor was replaced by a null row. This was done with the realistic as stated before. In the physical experimentation the connection to the sensor is removed to give a zero reading, the manipulator is allowed to function, and the corresponding joint response is plotted. As the sensor power was disconnected for the first joint, the revolute joint of the base link was unaffected and reached the steady state. However, the first joint could not reach the steady state. The prismatic joint of the base link failed to extend, and the magnitude of prismatic joint of the first link increased (i.e. the link extended) as the manipulator moved with the constant torque and force applied to the joints. The manipulator was able to reach the target, under control. The corresponding results are presented in Figure 4-3.

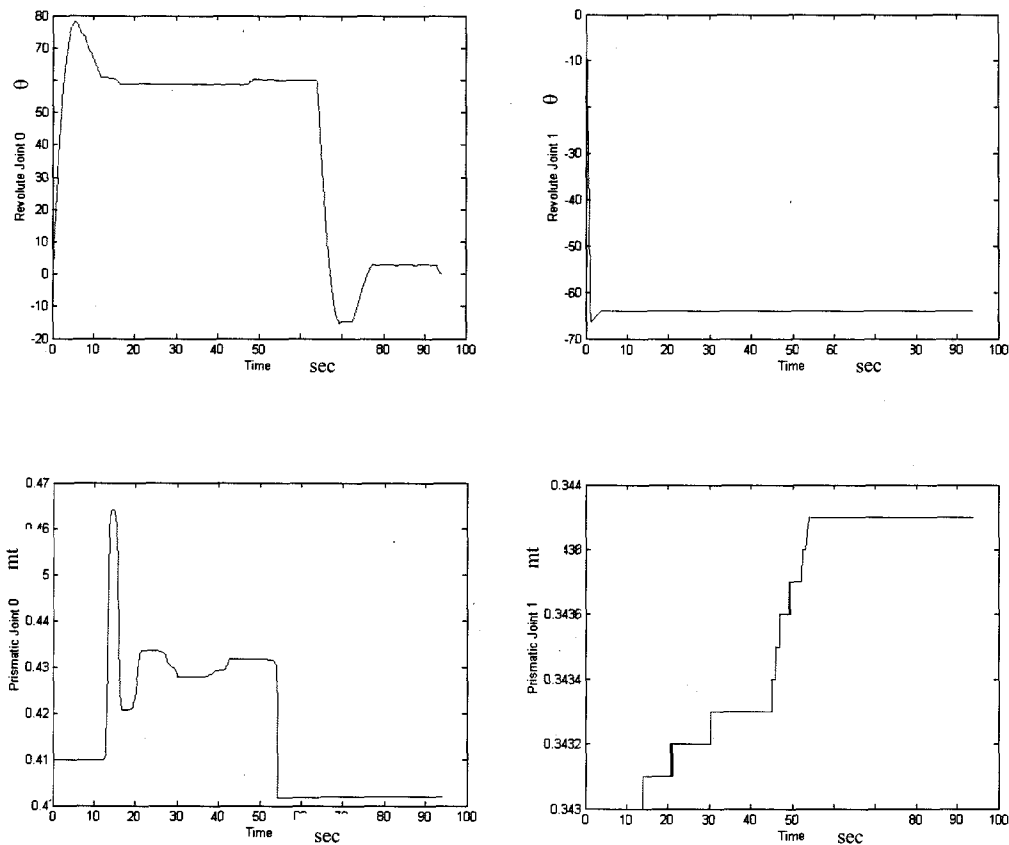


Figure 4-3: Manipulator Response Under Sensor Failure

It is observed that since the sensor failed for link 1, the rotational motion of link 1 could not achieve the target position. While the base link was operating in a normal manner, the prismatic joint extended with time as the manipulator operated. The joint adjusted and extended under control, to compensate for incorrect sensor reading, and reached the desired target point. The failure in sensor did not affect the speed of the controller and hence due to the availability of the redundant degree of freedom the manipulator was able to reach the target in the same time as in the normal operation scenario.

4.2.3 Locked Joint Failure

To implement the case of joint failure, the relative motion of a joint is stopped by some mechanism. This reduces the total number of degrees of freedom of the manipulator system by one. Once locked, the position of the locked joint stays the same as that at the instant just prior to the locking, while its relative velocity drops to zero and maintains the same value throughout the locked state.

In the present experiment, this case of failure is achieved by disconnecting the power to a particular joint motor while the braking is engaged. This represents a real state scenario where the power leads to a joint motor gets snapped due to some reason. The time response for this case is presented in Figure 4-4. There is an abrupt change in the velocity of the deployable base link at the instant the shoulder joint is locked; specifically, between the 15 to 30 sec period. The time delay corresponds to the disconnection of the power. However, the revolute joint of the first link is unaffected and functions in the normal fashion achieving the desired state. Though the velocity response attains the steady state, the base revolute joint gets locked at the instant the power is disconnected and stays in the same position for the rest of the cycle. During this stage the base prismatic joint tries to extend in the positive direction and then decreases as the moment of inertia of module 2 increases due to the extension of its deployable link. Through dynamic coupling, the shoulder joint rotates in the opposite direction to the elbow joint. Also the module moves at a slower pace because of the higher load and inertia, which it is driving. The locked shoulder joint fails to provide the torque to move the link and the manipulator fails to achieve the target.

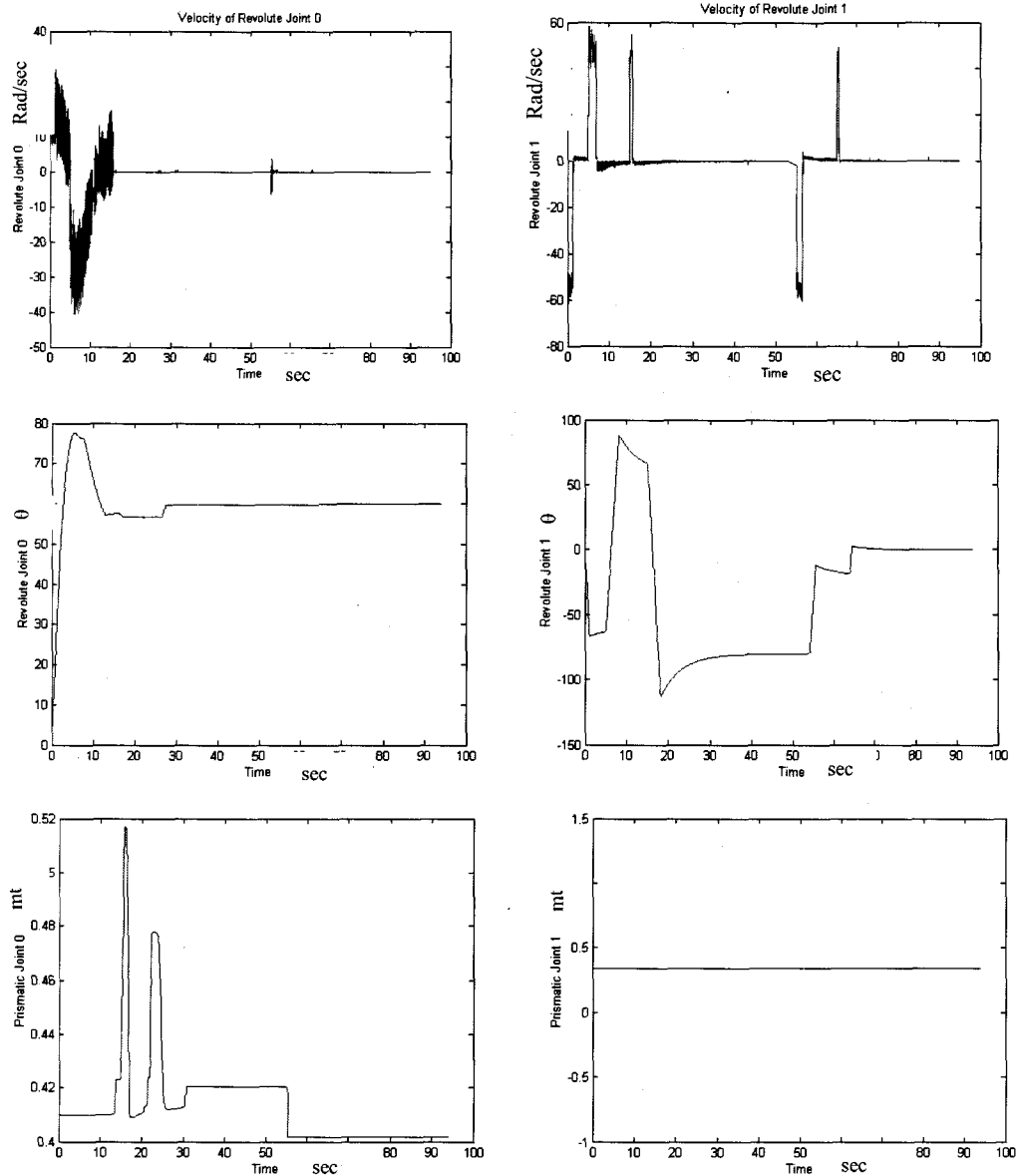


Figure 4-4: Manipulator Response Under Locked Joint

It is observed that when the failure occurs in the base revolute joint, then joint 1 tries to provide some compensation. However the prismatic joints fail to extend and achieve the target due to the increase of inertial force due to extension of the adjoining link. This is verified from the plot of the end effector trajectory of the manipulator, as shown in Figure 4-5. It is noticed that the tip failed to reach the target.

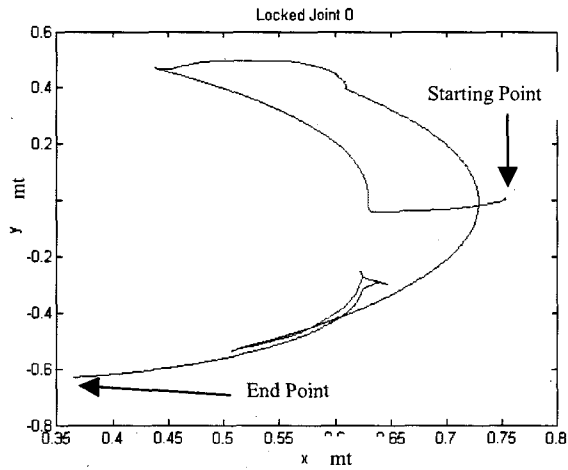


Figure 4-5: Trajectory of the Manipulator Tip

The same test was repeated while locking the shoulder joint. Similar results were obtained when joint 1 was locked, as seen in Figure 4-6. The prismatic joint extended to achieve the target as seen. However, the velocity response of base joint and joint 1 maintained equilibrium, and joint 1 extended to reach the goal position. The manipulator was unable to reach the target.

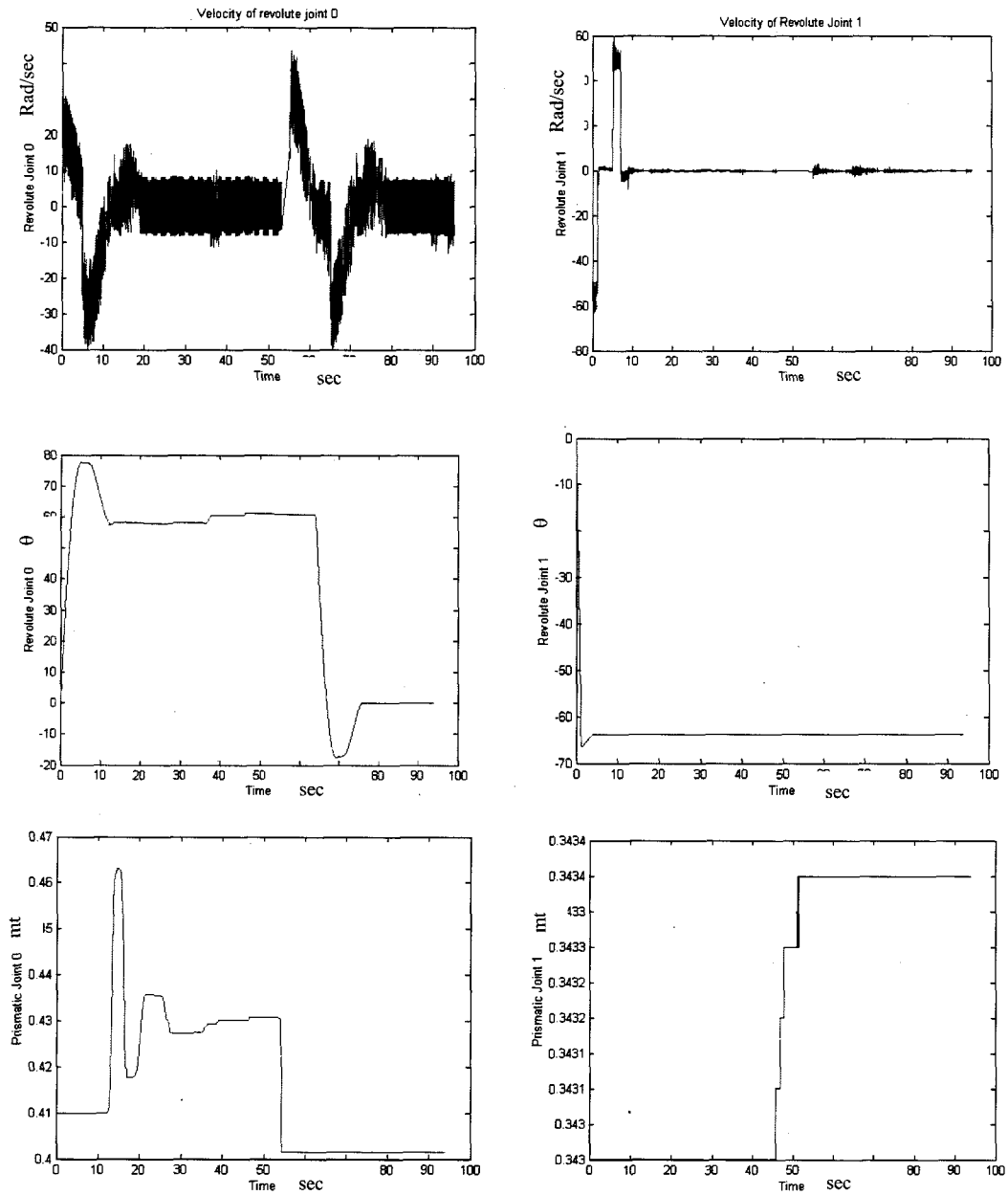


Figure 4-6: Manipulator Response Under Locked Joint 1

4.2.4 Free Wheeling Joint Failure

In the case of free-wheeling failure, we consider free swinging of a revolute joint. This could result from disconnection of gear engagement, breakage of a link or gear, slippage of transmission, or loss of connection between the motor and the link. All these failures result in the loss of torque in the actuator. As the actuator torque drops to zero, it fails to control the manipulator motion. In the experimental system this state is achieved by disconnecting the power to the actuator motor when the braking is not engaged. We observe that when the shoulder joint is set free, the movement of the shoulder becomes faster and it swings further in the negative direction. This is because a positive torque is not available to counteract the negative torque generated through dynamic coupling. The uncontrolled movement induces increased deployment and higher velocity in the base prismatic joint. As for joint # 1 in spite of the constant slew joint torque, the magnitudes of the position and velocity responses are larger. The results are presented in Figure 4-7.

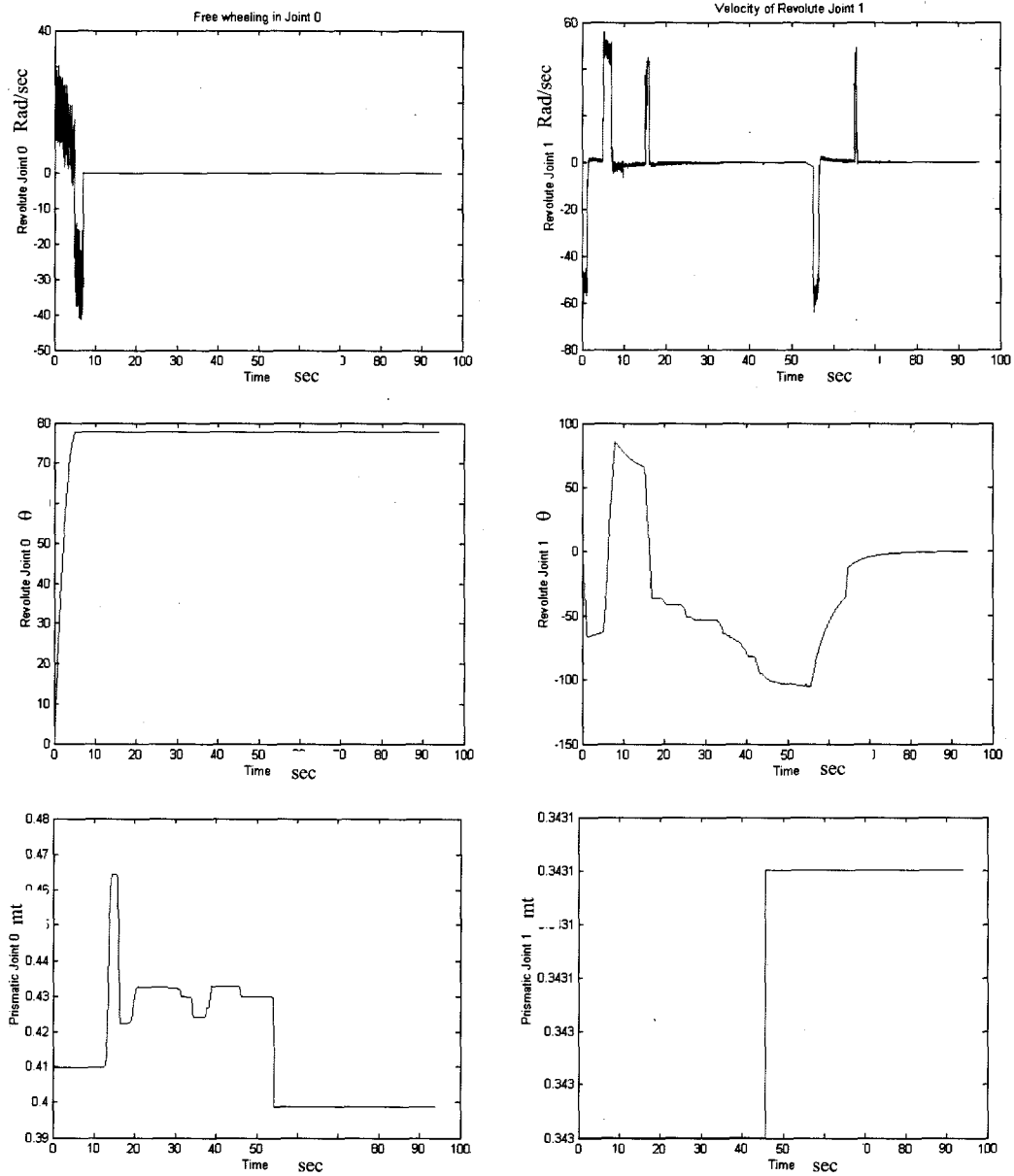


Figure 4-7: Manipulator Response Under Freewheeling of Base Link

As the revolute joint of the manipulator base loses its torque, joint 1 tries to achieve the equilibrium state and prismatic joint extends to reach the target. Prismatic joints function in the normal manner. In the absence of a positive torque the revolute joint fails to achieve the direction and there exists a free swinging of the base arm that swings further and faster in an uncontrolled manner in the negative direction. This faster motion induces an increased deployment and higher velocity in link 1. As expected in the absence of a positive torque, the manipulator fails to stay in control and fails to reach the target point. The final trajectory of the tip point is shown in Figure 4-8.

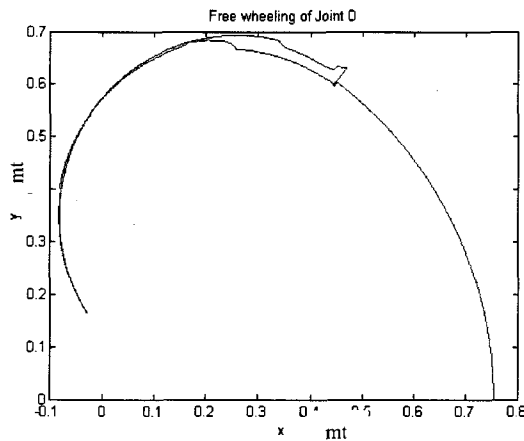


Figure 4-8: Tip Trajectory of the Manipulator

Similar results are obtained when the free swinging occurs in joint 1. The base revolute joint achieves the steady state; however, the negative torque in joint 1 causes free swinging of the arm. This response is shown in Figure 4-9.

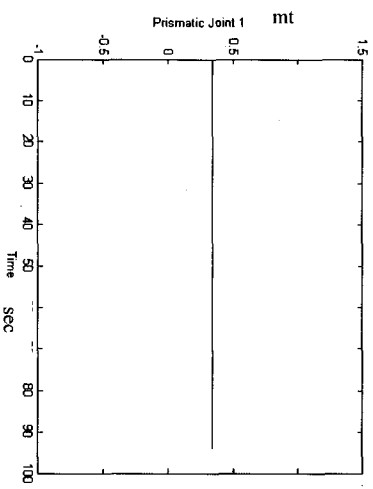
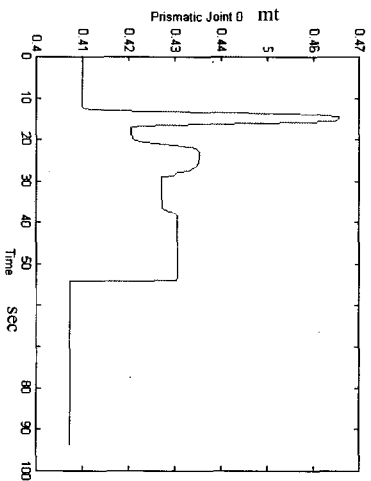
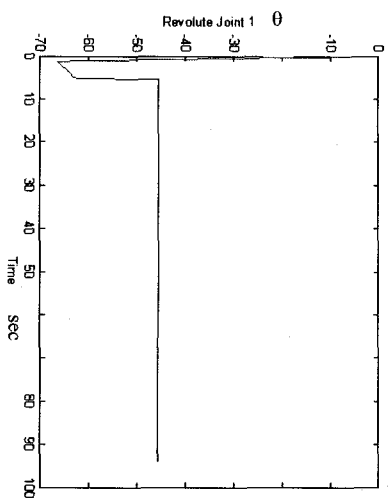
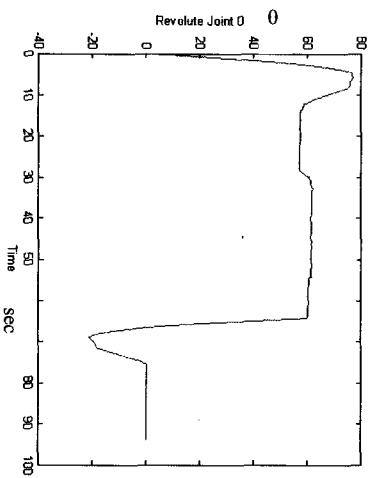
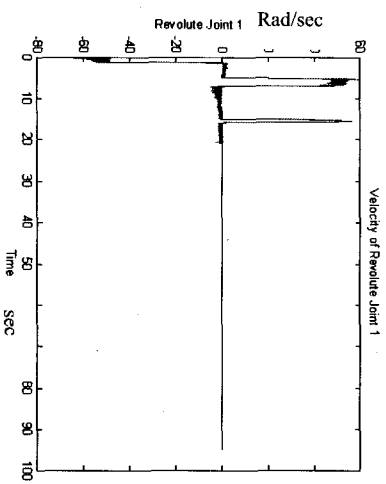
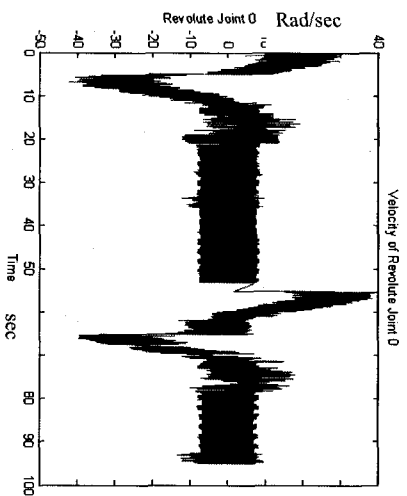


Figure 4-9: Manipulator Response Under Freewheeling of Joint 1

The traced path of the tip is shown in Figure 4-10. It is seen that due to the absence of a positive torque, the tip swings and the target is never achieved.

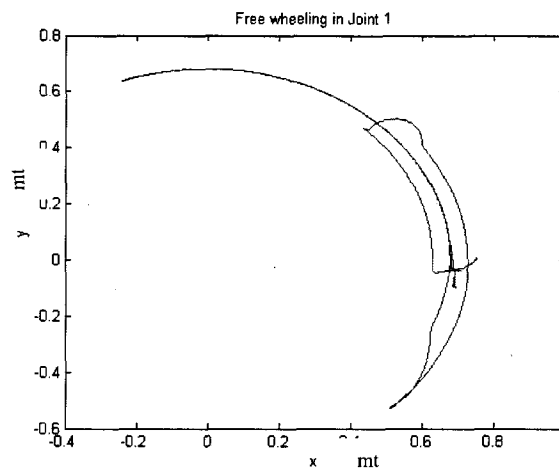


Figure 4-10: Tip Trajectory of the Manipulator

4.2.5 Prismatic Joint Locking Failure

The study is extended to carry out an experimental investigation when jamming of a prismatic link takes place so that it cannot extend or retrieve further. In a real life scenario this may result from jamming of the links due to additional friction generated on site due to bending of a link, dust collection, failure of the retracting motor or snapping of the power line to the motor. In the present experiments, this is achieved by disconnecting the power to the prismatic link motor. In particular, when the power supply to the base link prismatic joint is disconnected, it is observed that the revolute joint of the base and link 1 achieve steady state. The revolute joints move as a result of the applied constant torque and force. There is an abrupt change in the velocity of the base link approximately at 50 sec instant and reduces to zero. Link 1 extends to its deployable length and moves due to the inertial force, and due to the redundant degree of freedom the target is achieved, as shown in Figure 4-11.

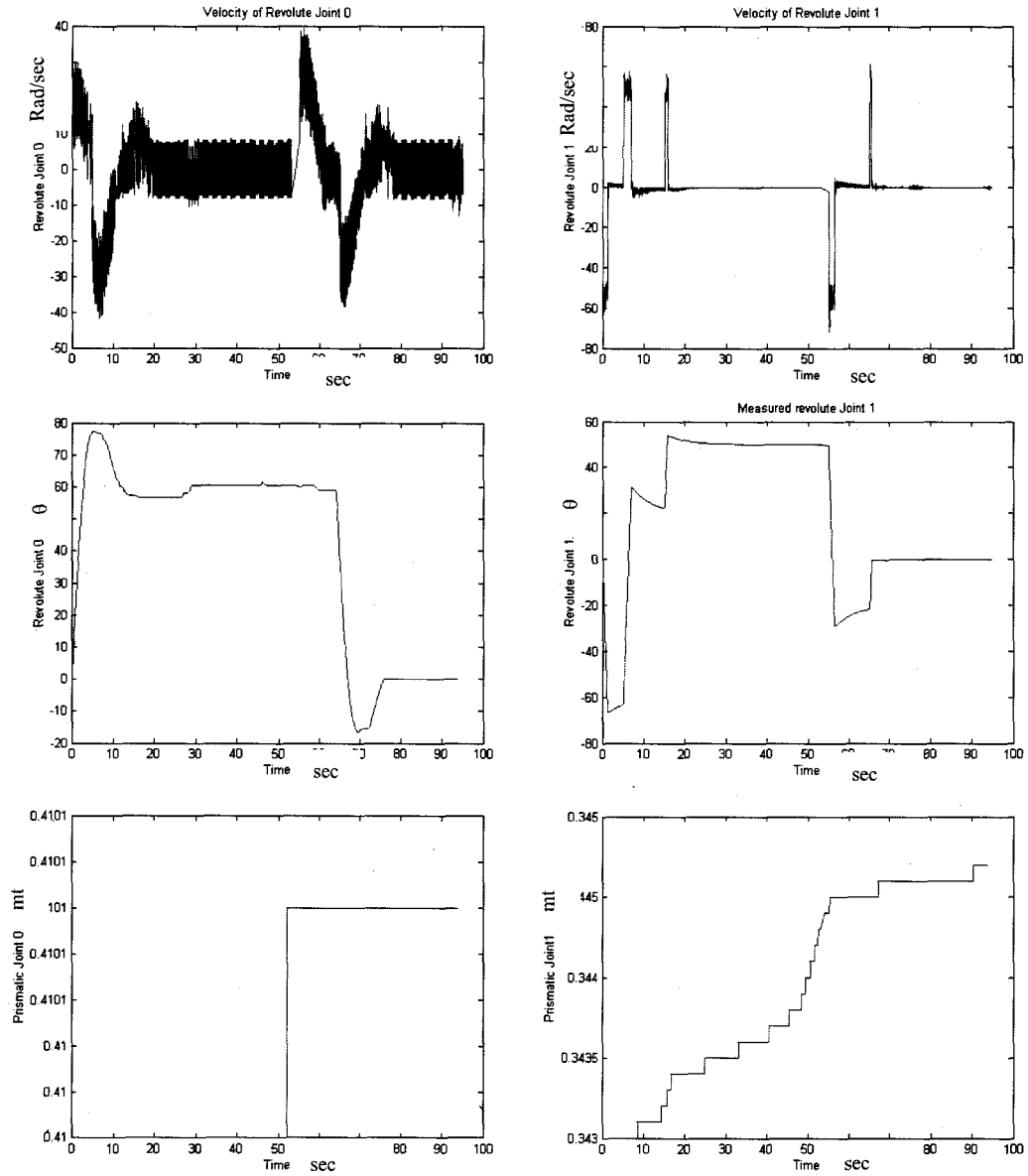


Figure 4-11: Manipulator Response Under Failure of the Base Link Prismatic Joint

The corresponding trip trajectory is shown in Figure 4-12. It is observed that the failure in one of the prismatic joints is accounted for and is compensated by the movements in the other link, and the tip achieves the target position.

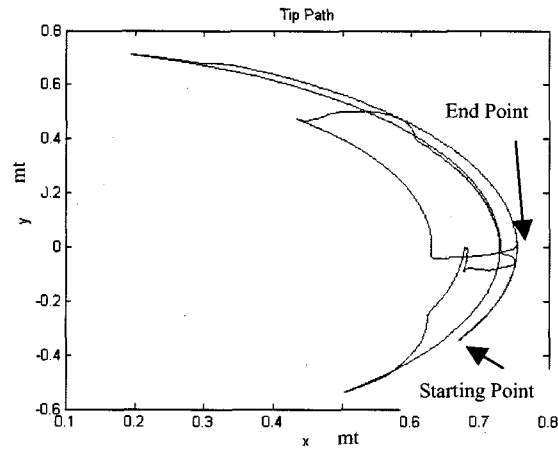


Figure 4-12: Tip Trajectory of the Manipulator

Similar experimental results were obtained when the prismatic joint of the second link was jammed. The corresponding responses of the manipulator are presented in Figure 4-13.

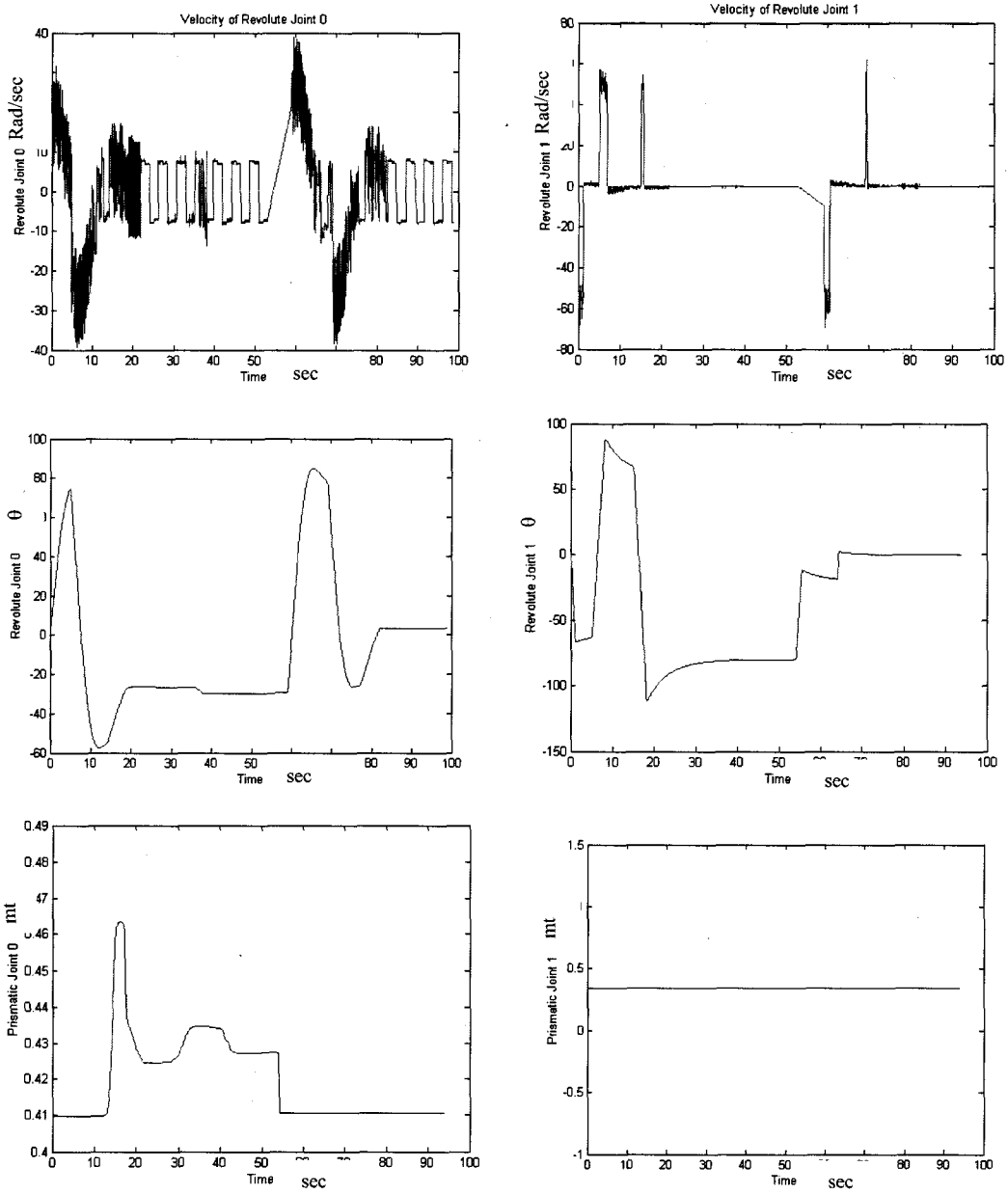


Figure 4-13: Manipulator Response Under Failure of the Prismatic Joint of Link 1

In this case link 1 has the fixed inertia. It is observed that all the slew movements achieve the steady state. The deployable length of base link compensates with its inertial force and the target is achieved. The tip trajectory plot shown in Figure 4-14 is similar to the results obtained in the previously.

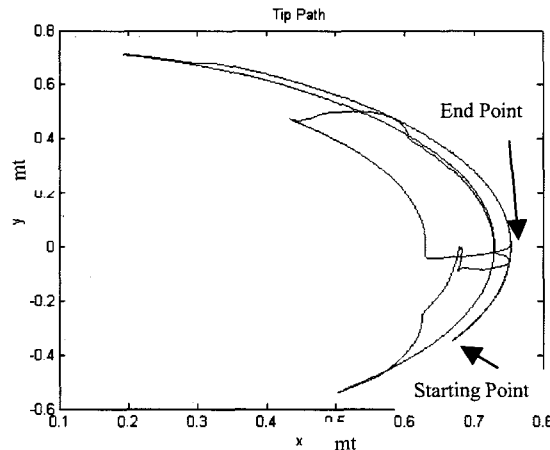


Figure 4-14: Tip Trajectory of the Manipulator

4.3 Discussion of the Results

The experimental results presented here are as obtained from the laboratory MDMS. It is observed that by and large, the failure detection scheme has performed satisfactorily.

Furthermore, in view of the availability of redundant kinematics in the MDMS, the manipulator has been able to complete a given task satisfactorily, under control, even in the presence of a joint failure or a sensor failure. These results verify the computer simulations as carried out previously [27]. In the simulation study, the manipulator achieved the target position with a joint locked. In the experimental investigation it was found to be true in the case of failure in a prismatic joint and sensor failure. The same was not found to hold, however, when a revolute joint (slew motion) failed. An inference can be made that if the direction is consistent, that is as long as the manipulator links have the right direction of motion, the target position can be reached under a joint failure. For this reason greater emphasis must be placed on the slew drives of the manipulator.

CHAPTER 5 CONCLUDING REMARKS

5.1 Significance of the Work

The present thesis focused on the study of failure detection and identification, and fault tolerant operation of an innovative multi-modular robot, the Multi-modular Deployable Manipulator System (MDMS), which has been designed and developed in our laboratory. In particular, Bayesian hypothesis testing was used to identify the failures in the MDMS. The work has a significant experimental component where the physical MDMS is subjected to several critical failure scenarios in our laboratory.

As the technology related to automatic control of robotic manipulators advance and as the required robotic tasks become increasingly critical and autonomous, the issue of reliability becomes more and more important. The ability to detect and identify a fault or a failure mode in a system and to continue the execution of the specified tasks in a satisfactory manner without the need for immediate human intervention is desirable. This calls for higher system reliability, better maintainability, improved survivability, increased efficiency, and greater cost effectiveness. Fault tolerant operation of robotic manipulators takes a centre stage in this context. In the present work various structural failure modes in a multi-module deployable manipulator system were studied through experimentation with a manipulator system developed in our laboratory. A methodology based on Bayesian hypothesis testing was implemented in the experimental robot, for on-line detection of a set of structural failures and sensor failure in the robot. The methodology was integrated into the control system of the manipulator so that, through the use of redundant kinematics, a faulty manipulator could operate satisfactorily in completing the assigned task, under certain situations. The experimental manipulator used in the present investigation has two modules, each having a revolute degree of freedom and a prismatic degree of freedom, to give a total of four degrees of freedom. In planar tasks of positioning and orientation, which require three degrees of freedom, the experimental robot has one degree of kinematic redundancy. It is this extra degree of freedom that is utilized in the fault tolerant operation of the manipulator under joint failure or sensor failure.

Past work on the subject has relied exclusively on computer simulation. The present work is particularly significant since it has involved implementation of an analytically sound strategy of failure identification into the control system of a sufficiently complex and practical manipulator system and using this manipulator for experimental investigation of the techniques of fault identification and fault tolerant operation.

5.2 Main Contributions

In the present work, Bayesian hypothesis testing that uses minimization of a cost function to identify a faulty condition, and a bank of Kalman filters for the estimation of fault-conditioned response were implemented in the control system of an innovative practical robotic manipulator. The experimental manipulator has been designed and developed in our laboratory (Industrial Automation Laboratory—IAL) of the University of British Columbia. The manipulator, MDMS, was intended for research in space-based applications of robotics, in view of the involvement of Canada in the development of the International Space Station (ISS) in cooperation with other countries. All the existing space based manipulators have exclusively revolute joints, providing rotational motions. However, our laboratory manipulator has combined revolute (rotational) and prismatic (translational) joints in each module. Several such modules are connected in series to form the MDMS, as desired. This innovative design has several advantages when compared with its counterparts with purely revolute joints and the same number of links. The main advantages are:

- Simpler decision making requirements;
- Reduced inertia coupling or dynamic interaction;
- Better capability to avoid obstacles; and
- Reduced number of singular positions.

Fault tolerant operation is critical in autonomous applications in remote locations and under hazardous conditions, as in space-based applications.

In the current work the experimental robotic manipulator was tested under a set of realistic scenarios, as encountered in the field, under the conditions of failure in manipulator joints and joint sensors. The failure could result from snapping of the power leads, motor failure, gear failure, slippage of gear, jamming of joints or gears, collisions resulting in bending or breakage of links and joints, and so on.

The experimental robot consisted of two modules, each having a revolute joint and a prismatic joint, providing a total of four degrees of freedom. Only three degrees of freedom are needed, however, for positioning and orientation tasks on a plane; consequently the experimental robot has one redundant degree of freedom. This redundant kinematics is key to fault tolerant operation of the manipulator. It was observed that when there is a failure in the motor of the telescopic (deployable or prismatic) link, the manipulator managed to reach the target point with the remaining three degrees of freedom. The manipulator compensated for the loss of a degree of

freedom and reached the target in a normal manner, under the command of its control system. Similar results were obtained for operation under sensor failure.

In the case of a slew (revolute) joint failure, it was observed that though there was a redundant degree of freedom available to assist the manipulator, the manipulator failed to reach the target location. This was due to the counter-productive torque produced in the system. The manipulator swung in an uncontrolled manner, in the absence of the necessary torque to counter it and bring the manipulator under control. Similar results were obtained when the revolute joint was locked. In this case manipulator did not swing; however, the manipulator failed to reach the target. The reason is the same as before; there was no adequate torque to provide the necessary movement to the joint.

Contrary to the findings through computer simulation, the manipulator system is not to be relied upon in all situations. In the case of failure in a revolute, the manipulator link would swing in uncontrolled manner, and the manipulator would fail to achieve the target position. In the case of failure in a translatory (telescopic, deployable, prismatic) link, the manipulator was able to compensate for the failure and reach the target position. In summary, when the manipulator is able to position in the desired direction it achieves the goal. Specifically, if the revolute drive mechanism works satisfactorily, the manipulator will overcome a fault in another drive and reach the goal.

5.3 Summary and Conclusions

MDMS, which has been designed and developed in our laboratory, consists of a set of serially connected modules, each having a revolute joint and a prismatic link. A general methodology for failure detection and identification based on Bayesian hypothesis testing was developed and implemented in the control system of this unique deployable manipulator system. Based on Bayesian hypothesis testing and using a bank of Kalman filters, the methodology was able to accurately identify the structural failures and joint sensor failure in MDMS.

The MDMS has redundant kinematics. In particular, this planar manipulator system needs only three degrees of freedom for a positioning and orientation task. However, the two-module experimental manipulator has four degrees of freedom. The present study is used in experimental investigation to study the fault tolerant behaviour of the experimental manipulator, which uses on-line fault identification and compensation through redundant kinematics.

The response of the physical manipulator system was obtained experimentally and analysed on-line to determine possible presence of joint failure or sensor failure. If failure is present, by

correctly identifying it and using the Kalman filter output corresponding to the particular failure mode, the manipulator is commanded to complete the task, with compensation from the redundant degree of freedom and under proper feedback control.

Four failure scenarios were studied in the present experimental investigation, namely: sensor failure; free wheeling of a revolute joint; locking of a revolute joint; and locking in a telescopic joint. It was observed that in the case of failure in a revolute joint, possibly due to gear failure, gear slippage, dust accumulation, power failure, and so on, the manipulator system failed to reach the target and thus became unreliable. However, in the case of failure in a telescopic joint or sensor failure, the manipulator was able to properly compensate for it and accurately track a specified trajectory and reach the target position, with the functional degrees of freedom and under command of the manipulator control system. Significant dynamic coupling was observed in the presence of joint flexibility, faster manoeuvre, and larger point payloads. It can be concluded that even though the methodology of fault identification and control is quite effective, the manipulator system needs improvement in its revolute joints. For example, a back-up drive may be provided for each revolute joint, to work in synchronism so that the failure of one drive can be accommodated by the stand-by drive.

5.4 Recommendations for Future Work

The present work has been an experimental investigation, where an analytically sound method of fault identification was implemented in the control system of a laboratory manipulator system, and tested for several important fault scenarios. This was an extension to computer simulations that have been carried out in our laboratory. This main objective has been accomplished in the present thesis. The simulation results were verified for the most part; however, it was found that only in some scenarios the manipulator succeeded in correctly reaching the target position.

The experimental investigation utilized the MDMS, which has been designed and developed in our laboratory, which consists of a set of serially connected modules, each having a revolute joint and a prismatic link. The present study was done using only two modules of manipulators, with a total of four degrees of freedom. Apart from the failure conditions studied in the present work, there are various other causes such as gear failure, increased backlash, motor failure, jamming of gears or links due to increased friction, bending of links, dust accumulation, and so on. It is important to further investigate the outcomes for various other types of failure and the behaviour of the manipulator under those conditions. While conducting the tests, utmost care must be taken as it can result in damage to the manipulator. It must also be noticed that the tests were carried

out in the horizontal plane with support provided by rollers. This mimics the zero gravity situation and is similar to application in space. However, further investigation may be done without the supports, as the links even though rigid, must be able to overcome the bending moment at each joint due to further links and dynamic coupling.

In summary, there are several issues that remain to be studied and demands further investigation, as listed below:

- I. As a future investigation, one may perform experiments with more than two manipulator modules. This should lead to the exploration of other dynamic issues and stability considerations.
- II. Extension of the inverse kinematics algorithm to account for a larger number of modules or N modules in general.
- III. Implementation of other, probably more advanced control methodology to perform control studies and evaluate the performance of the manipulator.
- IV. The studies can be expanded to various other failure modes scenarios such as slip in joint coupling due to backlash, wear or actuator loading, high resistance to joint motion, increased vibration due to gear malfunction, actuators or bearings, data acquisition failure, and so on. However, before such study is undertaken it is necessary to weigh the possible damage to the prototype manipulator, as the necessary repairs could be quite costly and time consuming.
- V. Further studies can be conducted by studying the manipulator without roller supports. The rollers in the present experimental set up provide support and counter-bending moment at each joint. However, if there are more units connected together, then the weights of the links will add to the bending moment and will load each consecutive drive mechanism, thus generating coupling dynamic forces, which need to be overcome.
- VI. Multiple failure modes can be applied simultaneously to the manipulator and the results studied. The present method of fault identification will have to be modified, or the number of hypotheses has to be correspondingly increased, in this case. For example, the failure of two degrees of freedom simultaneously may be studied in this manner.

BIBLIOGRAPHY

1. Alekseev, Y.K., Kostenko, V.V., and Shumsky, A.Y., "Use of Identification and Fault Diagnostic Methods for Underwater Robotics," *Proceedings of OCEANS '94 Oceans Engineering for Today's Technology and Tomorrow's Preservation*, San Diego, California, U.S.A., Vol. 2, pp 489-494, September 13-16, 1994.
2. Anderson, T.W., *An Introduction to Multivariate Statistical Analysis*, John Wiley & Sons, New York, NY, 1984.
3. Cao. Y., Dynamics and Control of Orbiting Deployable Multimodule Manipulators, M.A.Sc. Thesis, Department of Mechanical Engineering, University of British Columbia, Vancouver, Canada, pp. 8-13, 1999.
4. Cao. Y., Modi, V.J., de Silva, C.W., and Misra, A.K., "On the Control of a Novel Manipulator with Slewing and Deployable Links," *50th International Astronautical Congress, Amsterdam, Netherlands*, Paper No. IAF-99-A.5.06, 1990.
5. Caron M., Planar Dynamics and Control of Space-based Flexible Manipulators with Slewing and Deployable Links, M.A.Sc. Thesis, Department of Mechanical Engineering, University of British Columbia, Vancouver, Canada, pp. 111-115, 1994.
6. Caron, M., Modi, V.J., Pradhan, S., de Silva, C.W., and Misra, A.K., "Planar Dynamics of Flexible Manipulators with N Slewing Deployable Links," *Proceedings of the AIAA/AAS Astrodynamics Conference*, San Diego, California, U.S.A., AIAA Publisher Paper No AIAA-96-3625-CP, pp. 491-505, July 1996; also *Journal of Guidance, Control, and Dynamics*, Vol. 21, No. 4, pp. 572-580, July-August 1998.
7. Chen, Y., On the Dynamics and Control of Manipulators with Slewing and Deployable Links, Ph.D. Thesis, Department of Mechanical Engineering, University of British Columbia, Vancouver, Canada, 1999.
8. De Silva, C.W., "Recursive Linearizing and Decoupling Control of Robots," *Journal of Dynamics and Control*, Vol. 2, pp. 401-414, 1992.
9. De Silva, C.W., "Trajectory Design for Robotic Manipulators in Space Applications," *Journal of Guidance, Control, and Dynamics*, Vol. 14, No. 3, pp. 670-674, June 1991.
10. De Silva, C.W. and MacFarlane, A.G.J., "Knowledge-Based Control Approach for Robotic Manipulators," *International Journal of Control*, Vol. 50, No. 1, pp. 249-273, 1989.
11. De Silva, C.W., Wong, K.H., and Modi, V.J., "Design Development of a Prototype Multi-module Manipulator," *Proceedings of the IEEE/ASME International*

Conference on Advanced Intelligent Mechatronics (AIM 2003), Kobe, Japan, pp. 1384-1389, July 2003.

12. Goel, P., Dedeoglu, G., Roumeliotis, S.I., and Sukhatme, G.S., "Fault Detection and Identification in a Mobile Robot using Multiple Model Estimation and Neural Network," *Proceedings of the 2000 IEEE International Conference on Robotics & Automation*, San Francisco, California, U.S.A, Vol. 3, pp. 2302-2309, 24-28 April 2000.
13. Hokamoto, S., Kuwahara, M., Modi, V.J., and Misra, A.K., "Formulation and Control of Space-Based Flexible Robots with Slewing-Deployable Links," *Acta Astronautica*, Vol. 42, No. 9, pp. 519-531, 1998.
14. Hokamoto, S. and Modi, V.J., "Nonlinear Dynamics and Control of a Flexible Space-Based Robot with Slewing-Deployable Links," *Proceedings of the International Symposium on Microsystems, Intelligent Materials and Robots*, Sendai, Japan, Editors: J. Tani and M. Esashi, pp. 536-539, September 1995.
15. Hokamoto, S. and Modi, V.J., "Formulation and Dynamics of Flexible Space Robots with deployable Links," *Transactions of the Japan Society for Mechanical Engineers*, Vol. 62, No. 596, pp. 1495-1502, 1996.
16. Hokamoto, S., Modi, V.J., and Misra, A.K., "Dynamics and Control of Mobile Flexible Manipulators with Slewing and Deployable Links," *AAS/AIAA Astrodynamics Specialist Conference*, Halifax, Nova Scotia, Canada, Paper No. AAS-95-322; also *Advances in the Astronautical Sciences*, AAS Publications Office, San Diego, California, U.S.A., Editors: K. Terry Alfriend et al., Vol. 90, pp. 339-357, August 1995.
17. Karray, F.O. and de Silva, C.W., *Soft Computing and Intelligent Systems Design-Theory, Tools and Applications*, Addison Wesley, New York, NY, 2004.
18. Kimura, S., Takahashi, M., Okuyama, T., Tsuchiya, S., and Suzuki, Y., "A Fault-Tolerant Control Algorithms Having a Decentralized Autonomous Architecture for Space Hyper-Redundant Manipulators," *IEEE Transactions on Systems, Man and Cybernetics – part A; Systems and Humans*, Vol. 28, No. 4, pp. 521-528, July 1998.
19. Marom, I. and Modi, V.J., "On the Dynamics and Control of the Manipulator with a Deployable Arm," *AAS/AIAA Astrodynamics Specialish Conference*, Victoria, B.C., Canada, Paper No. AAS-93-670; also *Advances in the Astronautical Sciences*, Editors: A.K. Misra et al., Univelt Incorporated Publisher for the American Astronautical Society, San Diego, U.S.A, Vol. 85, Part III, pp. 2211-2229, August 1993.
20. Meditch, J.S., *Stochastic Optimal Linear Estimation and Control*, McGraw-Hill Book Company, New York, 1969.

21. Modi, V.J., Chen, Y., Misra, A.K., de Silva, C.W., and Marom, I., "Nonlinear Dynamics and Control of a Class of Variable Geometry Mobile Manipulators," *Proceedings of the Fifth International Conference of Adaptive Structures*, Sendai, Japan, Editor: J. Tani et al., Technomic Publishing Co. Inc., Lancaster, PA, USA, pp 140-149, December 1994.
22. Pradhan, S., Modi, V.J., and Misra, A.K., "Order N Formulation for Flexible Multibody Systems in Tree Topology – the Lagrangian Approach," *Proceedings of the AIAA/AAS Astrodynamics Conference*, San Diego, California, U.S.A., AIAA publisher, Paper no. AIAA-96-3624-CP, pp. 480-490, July 1996; also *Journal of Guidance, Control and Dynamics*, Vol. 20, No. 4, pp. 665-672, July-August 1997.
23. Shin, J.H., Lee, C.Y., and Lee, J.J., "Robust Fault-Tolerant Control Framework for Robotic Manipulators with Free-Swinging Joint Failures: Fault Detection, Identification and Accommodation", *Proceedings of the 1999 IEEE/RSJ International Conference on Intelligent Robotics and Systems*, Kyongju, Korea, Vol. 1 pp. 185-190, 17-21 October 1999.
24. Spong, M.W., "Modeling and Control of Elastic Joint Robots," *Journal of Dynamic Systems, Measurement and Control*, Vol. 109, pp. 310-319, December 1987.
25. Ting, Y., Tosunoglu, S., and Tesar, D., "A control Structure for Fault-Tolerant Operation of Robotic Manipulators," *Proceedings of the 1993 IEEE International Conference on Robotics and Automation*, Atlanta, Georgia, U.S.A., Vol. 3, pp 684-690, May 2-6, 1993.
26. Wong, H.K.K., Design, Integration and Dynamical Model of a Multi-module Deployable Manipulator System (MDMS), M.A.Sc. Department of Mechanical Engineering, Thesis, University of British Columbia, Vancouver, Canada, pp. 46-71, 1997.
27. Wong, H. K. K., "Structural Failure Identification and Control of the Multi-Module Deployable Manipulator System", Ph.D. Thesis, Department of Mechanical Engineering, University of British Columbia, Vancouver, Canada, April 2006.
28. Zhang, J., Modi, V.J., de Silva, C.W., and Misra, A.K., "An Assessment of Flexibility Effects for a Novel Manipulator," *Proceedings of the Eighth International Conference of Pacific-Basin Societies*, Xi'an, China, Editor: K.T. Uesugi et al., Chinese Society of Astronautics Publisher, pp. 22-26, June 1999.

APPENDIX I

Numerical data for the parameter values of the experimental manipulator (MDMS) used in the present investigation are listed below:

- Slewing link length, $l_s = 0.29$ m
- Deploying link length, $l_d = 0.18$ m
- Slewing link linear mass density, $\rho_s = 3.21$ kg/m
- Deploying link linear mass density, $\rho_d = 1.122$ kg/m
- Revolute joint actuator mass:
 - Module #1: $m_{a1} = 3.6$ kg
 - Module #2: $m_{a2} = 0.78$ kg
 - Module #3: $m_{a3} = 0.51$ kg
 - Module #4: $m_{a4} = 0.31$ kg
- Revolute joint actuator inertia:
 - Module #1: $J_{a1} = 1.2$ kg.m²
 - Module #2: $J_{a2} = 0.0816$ kg.m²
 - Module #3: $J_{a3} = 0.043$ kg.m²
 - Module #4: $J_{a4} = 0.015$ kg.m²
- Revolute joint stiffness:
 - Module #1: $K_1 = 10000$ Nm/rad
 - Module #2: $K_2 = 8830$ Nm/rad
 - Module #3: $K_3 = 1823$ Nm/rad
 - Module #4: $K_4 = 712.3$ Nm/rad